Subtilases turn on Pectin Methylesterase activity for a robust apoplastic immunity

Daniele Coculo[1], Daniele Del Corpo[1], Miguel Ozáez Martínez[2], Pablo Vera[2], Gabriella Piro[3], Monica De Caroli[3] and Vincenzo Lionetti[1, 4]*.

* Address correspondence to Vincenzo Lionetti (vincenzo.lionetti@uniroma1.it)

Keywords: Pectin Methylesterases, Subtilases, Plant Immunity, *Botrytis cinerea*, *Arabidopsis thaliana*, Cell Wall Integrity

1 Dipartimento di Biologia e Biotecnologie Charles Darwin, Sapienza Università di Roma, Rome, Italy

2 Instituto de Biologia Molecular y Celular de Plantas, Universidad Politecnica de Valencia-C.S.I.C, Ciudad Politecnica de la Innovacion, Valencia, Spain.

3 Dipartimento di Scienze e Tecnologie Biologiche e Ambientali, Università del Salento, Lecce, 73100 Italy

4 CIABC, Sapienza Università di Roma, Rome, Italy

One sentence Summary: Subtilase arm pectin methylesterase activity against pathogens to switch on pectin integrity signaling and to reinforce plant immunity to avoid the growth-defense trade-off

Running title: Subtilases arm PME activity in plant immunity

Abstract

Plants involve a fine modulation of pectin methylesterase (PME) activity against microbes. PME activity can promote the cell wall stiffening and the production of damage signals able to induce defense responses. However, to date, the knowledge about the molecular mechanisms triggering PME activity during disease remains largely unknown. In this study, we explored the role of subtilases (SBTs), serine proteases consisting of 56 isoforms in *Arabidopsis thaliana*, as activators of PME activity in plant immunity. By using biochemical and reverse genetic approaches, we found that SBT3.3 and SBT3.5 are required to control PME activity and resistance to the fungus *Botrytis cinerea. Arabidopsis sbt3.3 and sbt3.5* knockout mutants showed a reduced induction of PME activity and an increased susceptibility to *B. cinerea*. SBT3.3 expression is controlled by the damage-associated molecular patterns Oligogalacturonides. The SBT3.3 overexpression overactivates PME activity only during fungal infection resulting in an increased expression of the defense-related genes and in an enhanced resistance to *B. cinerea*. We revealed that SBT3.3 and the Pro-PME17 isoforms are both secreted in the cell wall using a conventional protein secretion pathway and their colocalization in the apoplast increase over time. Our findings point to SBTs as a mechanism to switch on pectin integrity signaling and to reinforce plant immunity at the right time to avoid the growth-defense trade-off.

Introduction

Plants continuously perceive attacks by microorganisms activating a timely and effective immune response. Part of this recognition is exerted by plasma membrane Pattern Recognition Receptors (PRRs), which can detect Microbe-, Pathogen-, or endogenous Damage Associated Molecular Patterns (MAMPs, PAMPs or DAMPs)(Zhou and Zhang, 2020). Pattern-triggered immunity (PTI) constitutes the first line of plant inducible immunity that restricts pathogen proliferation. Since the immunity efforts often result in a growth defense trade-offs, a precise regulation of immune pathways becomes critical to optimize fitness (Lionetti et al., 2010; Huot et al., 2014; Ha et al., 2021). A pivotal role in this homeostasis is played by proteolysis mediated by proteases, widely implicated in plant stresses, although their action mechanisms remain largely unknown (Schaller, 2004; Hou et al., 2018). In particular, Subtilases (SBTs, Pfam00082), serine peptidases belong to family S8, (MEROPS database; https://www.ebi.ac.uk/merops/cgi-bin/famsum?family=S8) plays key roles in defense responses against microbes, plant parasitism and adaptation to the environmental changes (Figueiredo et al., 2018; Schaller et al., 2018; Ogawa et al., 2021). In *A. thaliana*, 56 SBT isoforms are divided into 6 subfamilies: SBT1, SBT2, SBT3, SBT4, SBT5, SBT6 (Rautengarten et al., 2005).

Specific SBTs are targeted to the plant Cell Wall (CW), the foremost interface at which interactions between plants and microbes take place, to trigger specific protease-activated defense signaling (Doehlemann and Hemetsberger, 2013). In this compartment, SBTs can process larger precursor zymogens (Pro-Proteins), that require specific activation processes for enzyme maturation (Khan and James, 1998). SBT6.1 (S1P) can process the pro-peptide form of RAPID ALKALINIZATION FACTOR 23 (RALF23) modulating immune response against *Pseudomonas syringae* (Stegmann et al., 2017). In tomato, specific SBTs contributes to Jasmonic Acid-mediated resistance against *Manduca sexta* larvae, by processing the wound pro-hormone Prosystemin, releasing the bioactive peptide called Systemin (Meyer et al., 2016). The six genes of the tomato cluster SBT P69 (P69A–P69F) express proteins particularly involved in plant defense. P69B can cleave the *Phytophthora infestans* PC2, a cysteine-rich secreted apoplastic protein releasing immunogenic peptides that activates host immunity (Wang et al., 2021). In particular, P69C processes an extracellular matrix-associated Leucine-Rich Repeat protein (LRP), the first physiological target of an extracellular SBT identified in plants (Tornero et al., 1996). SBT3.3, the ortholog of tomato P69C in *Arabidopsis*, was discovered as regulator of *Arabidopsis* primed immunity (Ramirez et al., 2013). Although SBT3.3 was postulated to cleave an

extracellular larger protein, the identification of its specific substrate and the mechanism by which SBT3.3 can trigger immunity remains to be identified.

During plant development, specific SBTs can process specific Pectin Methylesterases (PME; Pfam01095), enzymes regulating the methylesterification of Homogalacturonan (HG), the major constituent of pectin in the CW (Wormit and Usadel, 2018; Coculo and Lionetti, 2022). PMEs catalyse the hydrolysis of methylester bonds at C-6 of Galacturonic Acid (Gal A) residues, producing acidic pectins with negatively charged carboxyl groups, releasing methanol (MeOH) and protons into the apoplast. In *Arabidopsis*, 66 PME isoforms have been identified which can be classified into 2 groups on the basis of their structures (Pelloux et al., 2007; Dedeurwaerder et al., 2008). Group 1 comprises 21 PME isoforms, containing only the catalytic domain. The 45 PME isoforms of Group 2 (hereafter named Pro-PMEs) are organized as a polycistronic messenger RNA which resembles an operon-like gene cluster (Coculo and Lionetti, 2022). In Pro-PMEs, the PME catalytic domain is preceded by an N-terminal region (also referred as Pro region or PMEI-like domain) which shares structural similarities with functionally characterized PME Inhibitors (PMEIs) and that can acts as auto-inhibitor of PME activity (Bosch et al., 2005; Wolf et al., 2009; Del Corpo et al., 2020). This domain could impede a premature pectin de-methylesterification, during specific phases of their secretion, assembly, or modification contributing to a correct pectin functionality.

A local and strong induction of PME activity is exerted in *Arabidopsis thaliana* and other plants, when challenged with different microbial pathogens (Bethke et al., 2014; Lionetti, 2015; Lionetti et al., 2017). *Pro-PME17* isoform is strongly upregulated in response to several pathogens, defense hormones, elicitors or abiotic stress and its activity strongly contribute to the induction of defense-related PME activity (Bethke et al., 2014; Del Corpo et al., 2020). A finely tuned PME activity can play multiple functions in plant immunity. PMEs can produces de-methylesterified negatively charged carboxyl groups that can form consecutive calcium bonds with other HG molecules and thus strengthen the CW through the formation of “egg-boxes” structures (Senechal et al., 2014b; Del Corpo et al., 2020). Plant PME activity can also favour DAMP related immunity. In particular, the PME activity could favour the release and perception of de-methylesterified oligogalacturonides (OGs), the well characterized DAMP, locally released in cooperation with endo-polygalacturonases (PGs), and able to trigger plant immunity (Osorio et al., 2008; Osorio et al., 2011; Ferrari et al., 2013; Kohorn et al., 2014). OGs are perceived in *Arabidopsis* by the pathogen recognition receptor WALL-ASSOCIATED KINASE1 (WAK1) to activate plant immune responses (Brutus et al., 2010; Kohorn

and Kohorn, 2012). WAK2 requires PME-mediated pectin de-methylesterification to activate OGs-dependent stress responses (Kohorn et al., 2014). Interestingly, WAK1, WAK2 and another PRR, FERONIA (FER), preferentially bind to de-methylesterified pectins (Decreux and Messiaen, 2005; Kohorn et al., 2014; Feng et al., 2018; Guo et al., 2018; Lin et al., 2021). The de-methylesterification of pectin by PMEs represents the main mechanism to generate plant-derived methanol (MeOH), a DAMP-like alarm signal (Hann et al., 2014). OGs and MeOH are able to trigger defensive priming effect setting the stage for the intra and inter-plant immunity (Dorokhov et al., 2012; Komarova et al., 2014; Gamir et al., 2021; Giovannoni et al., 2021).

Precise switch on/off mechanisms regulating PME related immunity are required because they must be timely triggered for an efficient immune response and they cannot be persistent given the well-known defense growth trade-off (He et al., 2022). The need of a post-transcriptional control of PME activity by specific PME inhibitors (PMEIs) late during plant invasion by microbes was previously demonstrated (An et al., 2008; Lionetti et al., 2017; Liu et al., 2018). The involvement of SBTs as posttranscriptional processing of Pro-PMEs and regulation of PME activity in plant immunity was still not investigated. Here, we found that all the PME isoforms induced in *A. thaliana* against the necrotrophic fungus *Botrytis cinerea* possess a Pro-region. Exploiting reverse genetic approaches and biochemistry, we demonstrated that SBT3.3 and SBT3.5 contribute to the induction of PME activity in *Arabidopsis* immunity against *Botrytis*. Notably, we found that SBT3.3 processes defense-related Pro-PMEs as substrate and trigger specific defense related genes. SBT3.3 follows a conventional secretion pathway to reach the apoplast where colocalizes with Pro-PME17. Our results provide strong evidence that the processing of Pro-PMEs by SBTs represents a mechanism to switch on pectin integrity signaling for a timely immune response to avoid a growth-defense trade-offs.

RESULTS

The processing of Pro-PME zymogens is required in *Arabidopsis-Botrytis* interaction

PMEPCRA, *PME3*, *PME17*, *PME20*, *PME21*, and *PME41* are the PME isoforms exhibiting a significant altered timing and level of expression in *A. thaliana* - *B. cinerea* interaction and in several other pathosystems (Lionetti et al., 2012; Bethke et al., 2014; Lionetti et al., 2017). Interestingly, after a careful comparison of the sequences we realized that all these isoforms are zymogens, expressed as Pro-PME inactive precursors (Supplemental Figure S1). This strongly suggest that a proteolytic cleavage, exerted by specific proteases, is requested for PME activation in *Arabidopsis* immunity

against *Botrytis*. While the PME catalytic domain is highly conserved, we intriguingly noticed here a variability in the processing motif between the different PME isoforms. Pro-PMEPCRA, Pro-PME17 and Pro-PME21 showed a RKLL processing motif, while the RRKL motif characterized the Pro-PME20 and Pro-PME41 isoforms. Instead, two processing motifs, RKLK and RRLL were present in the Pro-PME3. Other motifs with the consensus sequence FPSW and LPLKMTERARAV are partially conserved between the isoforms. All these observations could imply the involvement of multiple proteases-PME pairs.

***SBT3.3* and *SBT3.5* are induced in *Arabidopsis* during *B. cinerea* as part of PTI**

We explored the possibility that SBTs are involved in the processing and activation of Pro-PMEs against microbes. Exploiting publicly available microarray data, we selected two genes, *SBT3.3* and *SBT3.5* showing a significative induction during *B. cinerea* infection (Supplemental Figure S2A). Interestingly, both genes are co-expressed with *Pro-PME17*, a functional PME involved in the resistance to *Botrytis cinerea* (Supplemental Figure S2B) (Lionetti et al., 2012; Del Corpo et al., 2020). To confirm the transcriptomic analysis and to gain more insight in the kinetic of expression of these genes during the disease, the expression levels of *SBT3.3* and *SBT3.5* were quantified at different times in *B. cinerea*-infected and Mock-inoculated *A. thaliana* wild type (WT) leaves by qPCR (Figure 1A and B). *SBT3.3* is expressed only in infected tissues while *SBT3.5* shows a basal expression also in Mock-inoculated leaves. *SBT3.3* and *SBT3.5* were significantly induced at 24 hpi and further increased at 48 hpi, when they showed about a significant 15- and 5-fold induction, respectively, in infected leaves compared to Mock inoculated tissues. These data clearly reveal an involvement of *SBT3.3* and *SBT3.5* in *Arabidopsis-Botrytis* interaction. Interestingly, the expression of both *SBTs* is also triggered in *Arabidopsis* against several pathogens and by different bacterial and fungal elicitors of plant defense responses (Supplemental Figure S3). We next investigated whether pectin-related DAMPs can impact on the expression of the selected SBTs. *Arabidopsis* WT seedlings were treated with OGs or water, and the expression of *SBT3.3* and *SBT3.5* was evaluated at 1 h post treatment. A 7-fold induction of *SBT3.3* was revealed after treatment with OGs (Supplemental Figure S3 and Figure 1C), while the expression of *SBT3.5* was not induced (Supplemental Figure S3 and Figure 1D). All these results indicate that *SBT3.3* and *SBT3.5*, are part of *Arabidopsis* immune responses against *B. cinerea* and several pathogens.

SBT3.3 and SBT3.5 contribute to Arabidopsis PME activation and resistance to *B. cinerea*

To explore on the possibility that SBT3.3 and SBT3.5 may be involved in the activation of Pro-PMEs in plant immunity we exploited a reverse genetic approach. Two T-DNA insertional mutants for the selected genes were isolated (Figure 2A). The insertions were localized in the fifth and ninth exons, respectively, for *sbt3.3-1* (SALK_086092) and *sbt3.3-2* (SALK_107470.45.45) mutants and in the first exon and in the second intron, respectively for *sbt3.5-1* (SAIL_400_F09) and *sbt3.5-2* (GABI_672C08) mutants. The level of *SBT3.3* and *SBT3.5* expression was compared in leaves of mutants and WT plants after *B. cinerea* and Mock inoculation by qPCR (Figure 2B). All mutants fail to induce gene expression in fungus-challenged leaves, resulting in *SBT3.3* and *SBT3.5* KO lines. No significant defects were observed in the rosette growth and seed germination in *sbts* mutants which showed the growth parameters like WT plants (Figure 2C and S4A and B). To understand if the lack of SBTs expression can influence pectin composition we compared the monosaccharide composition of matrix polysaccharides extracted from rosette leaves of SBTs mutants and WT plants. All mutants analysed showed a molar percentage of monosaccharides not significantly different from that observed in WT plants (Figure 2D).

After establishing that the two subtilases are involved in *Arabidopsis-Botrytis* interaction we evaluated their possible contribution in the control of PME activity during fungal infection. The level of PME activity was quantified in leaves of WT, *sbt3.3-1*, *sbt3.3-2*, *sbt3.5-1* and *sbt3.5-2* plants at 24 hours post *Botrytis* and Mock inoculation using histochemical and biochemical assays based on Ruthenium Red (RR), a cationic dye with six positive charges able to bonds with the acidic groups of HG (Lionetti, 2015)(Figure 3A). A significant lower induction of PME activity was observed in infected *sbt3.3-1*, *sbt3.3-2*, *sbt3.5-1* and *sbt3.5-2* mutants (respectively of 3.7-, 3.1, 1.9- and 1.8-fold reduction) compared to WT (Figure 3B). These results unveil for the first time that Pro-PMEs are substrates for SBT3.3 and indicate that SBT3.3 and SBT3.5 contribute to control the PME activity in *Arabidopsis* immunity to *Botrytis*. Interestingly, the significant difference found in *sbt3.3* respect to *sbt3.5* mutants suggest that the two proteases can process different Pro-PMEs isoforms during disease. No significant differences in PME activity were observed between Mock-inoculated WT plants and *sbt* mutants. This was expected for *sbt3.3* mutants, as *SBT3.3* is not basally expressed in leaves (Figure 1A). In *sbt3.5* mutants, the lack of the basal *SBT3.5* expression in *Mock*-inoculated leaves (Figure 2B) does not significantly affect the monosaccharide composition and the total PME activity in leaves (Figure 2D and 3B) as well as on the rosette growth and seed germination (Figure 2C and Supplemental Figure S4). Therefore, we evaluated the susceptibility of *sbt3.3* and *sbt3.5* mutants to *B. cinerea* (Figure 4A

and B). The local symptoms of the fungus were significantly higher in both *sbt3.3* and *sbt3.5* mutants respect to WT. In particular, the lesion areas produced by the fungus were larger in *sbt3.3-1*, *sbt3.3-2*, *sbt3.5-1*, *sbt3.5-2* mutants (respectively, of 2.2-, 2.1, 1.7- and 1.7-folds) respect to WT. A greater development of *Botrytis* mycelium was detected in *sbt* mutants respect to WT plants using trypan blue staining (Figure 4B). All our results indicate that, although at different extent, both SBTs contribute to trigger PME activity and the resistance to *Botrytis*. A correlation between the level of resistance and the amount of PME activity expressed in the tissues were observed between the different genotypes analysed (Figure 3 and 4).

SBT3.3 overexpression over activates defense related PME activity restricting *Botrytis* infection

Given the lower induction of PME activity observed in *sbt3.3* mutants compared to those of SBT3.5, we deepen our study on SBT3.3 exploring the effect of its overexpression in *Arabidopsis* on PME activity and *Botrytis* resistance. Two transgenic *Arabidopsis* lines, named *SBT3.3-OE1* and *SBT3.3-OE2* exhibiting high level of SBT3.3 expression in leaves were characterized (Figure 5A). Interestingly, an 85- and 90-fold overexpression was revealed, respectively, in leaves of *SBT3.3-OE1* and *SBT3.3-OE2* lines respect to WT leaves when infected with *B. cinerea*. No growth abnormalities were observed in *SBT3.3* overexpressing plants (Figure 5B and S4). The CW monosaccharide composition in rosette leaves of SBT3.3-OE lines is not significantly different from that quantified in the WT plants (Figure 5C). These results are consistent with those obtained with the mutants and corroborate the conclusion that the expression of *SBT3.3* is dedicated to the *Arabidopsis* immune response. The level of PME activity was quantified in leaves of WT, *SBT3.3OE-1 and SBT3.3OE-2* plants at 24h post *Botrytis*- and Mock-inoculation (Figure 6A). A significant higher induction of defense-related PME activity was observed in the infected *SBT3.3* overexpressing lines compared to control. *SBT3.3OE-1* and *SBT3.3OE-2* lines showed, respectively, a 3.1- and 2.3- fold increase of PME activity in the *B. cinerea* infected leaves compared to WT. Despite the overexpression of *SBT3.3* in transgenic Mock-inoculated plants (Figure 5A), the level of PME activity were not significantly different from that measured in WT plants (Figure 6A). This result highlights that SBT3.3 trigger PME activity exclusively in *Arabidopsis* defense against the fungus. The levels of methylesters remained in plant cell wall after 24 h of *B. cinerea* inoculation were compared between *SBT3.3-OE* lines and WT plants. A significant lower amount of methylesters was revealed in the CW extracted from *B. cinerea* infected leaves of *SBT3-3-OE1* and *SBT3.3-OE2* lines respect the WT plants (Figure 6B). This result

confirms that SBT3.3 processes the Pro-PMEs in plant defense and that a higher PME activity was released by SBT3.3 overexpression in transgenic challenged with the fungus respect the control.

Next, we evaluated the susceptibility of *SBT3.3-OE* lines to *B. cinerea*. The local symptoms of the fungus were significantly lower in both *SBT3.3-OE* plants when compared with the WT (Figure 6C and D). In particular, the lesion area produced by the fungus in *SBT3.3-OE1* and *SBT3.3-OE2* mutants are 2- and 1.5-fold lower compared to WT. A minor development of *Botrytis* mycelium was detected in *SBT3.3-OE1* plants respect to WT plants using trypan blue staining (Figure 6D). All these results support an important role of SBT3.3 as trigger of PME activity in *Arabidopsis* immunity to Botrytis and indicate that the SBT3.3 overexpression confers to *Arabidopsis* a higher resistance to *B. cinerea* respect to WT.

SBT3.3 overexpression enhances immune responses against _Botrytis_

The next goal was to verify whether the improved resistance observed in the SBT3.3 overexpressing lines could be linked to a more robust immune response. The induction of an array of defense related genes important for *Arabidopsis* defense against *Botrytis* was compared between WT and *SBT3.3-OE1* plants inoculated with Mock and *Botrytis*. *WRKY33* is a key transcriptional regulator of hormonal and metabolic responses toward *B. cinerea* infection (Birkenbihl et al., 2012). *WRKY33* can targets the promoter of *PHYTOALEXIN DEFICIENT3 (PAD3)* encoding an enzyme required for the synthesis of antimicrobial camalexin (Zhou et al., 1999). The cytochrome P450 enzyme *CYP81F2* is essential for the pathogen-induced accumulation of 4-methoxy-indol-3-ylmethyl Glucosinolate (Clay et al., 2009; AbuQamar et al., 2017). *WAK2* is a wall associated kinase mediating pectin related immunity and activated by de-methyl esterified pectin to trigger defense responses (Kohorn et al., 2014). *PME17* and *PMEI10* are two regulators of PME activity in plant immunity to *B.cinerea* (Lionetti et al., 2017; Del Corpo et al., 2020). Interestingly, a higher induction of *WRKY33*, *PAD3*, and *WAK2* were observed in *SBT3.3-OE1* plants respect the WT only when challenged with the fungus (Figure 7). *CYP81F2* showed levels of expression similar between WT and *SBT3.3-OE1* plants. However, considering the lower level of *B.cinerea β-tubulin* and the lower fungal symptoms observed in transgenic plants (Figure 7 and Figure 6C and D) it is possible to conclude that CYP81F2 expression is stimulated by *SBT3.3* overxpression. Following the same reasoning, the *Pro-PME17* and *PMEI10* expressions are independent from SBT3.3 activity since their inductions follow the extent of fungal infection and *B.cinerea β-tubulin* expression. These findings indicate that SBT3.3 contribute to enhance Arabidopsis

immunity, most likely, improving the production of antimicrobial compounds and reinforcing cell wall integrity surveillance.

We next explored if SBTs expression can influence Hydrogen Peroxide production, an important defense response to *Botrytis* infestation (Pogorelko et al., 2013; Siegmund and Viefhues, 2016). Leaves of WT, *sbt3.3-1*, *sbt3.5-1* and *SBT3.3-OE1* plants, were inoculated with Mock or *B. cinerea* and stained with 3,3′-diaminobenzidine, a chromogen able to reveal the H_2O_2 accumulation in the tissue (Reem et al., 2016). No accumulation of H_2O_2 was observed in Mock-inoculated leaves of all genotypes analyzed and a similar DAB staining was revealed in all the leaves challenged with *Botrytis*. These results indicate that H_2O_2 production is not dependent from SBTs mediated signaling (Supplemental Figure S5).

SBT3.3 and Pro-PME17 are delivered through a conventional protein secretion pathway and colocalize in the apoplast

SBT3.3 was previously demonstrated to be an extracellular subtilase, but its secretion pathway was never explored (Ramirez et al., 2013). Moreover, Pro-PME17 was predicted as an apoplastic protein, but its localization was never demonstrated. With the aim to deepen our knowledge on the secretion patterns and the final subcellular destination of the two proteins, a fluorescent variant of SBT3.3 and of Pro-PME17 were constructed by fusing the respective encoding cDNA to *yfp* and *gfp*, under the control of *35S* promoters. The fluorescent tag was linked to the C-terminus, as none of the two protein is predicted to have the ω site of the glycosylphosphatidylinositol (GPI) anchor addition (predGPI software; http://gpcr2.biocomp.unibo.it/predgpi/), as previously found for AtPMEI1 (De Caroli et al., 2011). *SBT3.3-YFP* and *Pro-PME17-GFP* constructs, were transiently expressed in the epidermal cells of tobacco leaves and observed by laser scanning confocal microscopy (Figure 8). The fluorescence signals relative to both proteins, labelled the ER and the Golgi stacks as revealed by colocalization experiments using ER and Golgi markers *RFP-HDEL* and *ST52-mCherry* (Nelson et al., 2007) (Figure 8 A-F and K-P). Both proteins accumulate in the apoplast as confirmed by co-localization with the CW marker XTH11-RFP (De Caroli et al., 2021) (Figure 8 G-I, Q-S) and plasmolysis of epidermal cells co-expressing both *pm-rk*, marker of plasma membrane (Nelson et al., 2007) and *SBT3.3-YFP* or *Pro-PME17-GFP* (Figure 8 J, T). Intriguingly, the Pro-PME17 reaches the apoplast before the SBT. At 48 h post transformation, the CW was fluorescently labelled by Pro-PME17-GFP and after 52 h by SBT3.3-YFP protein fusion (Figure 8, B and E). These results indicate that that SBT3.3 and Pro-PME17 are

correctly secreted into the apoplast both using a conventional secretion pathway but in a temporally staggered manner. The compartment and timing of SBT3.3 and Pro-PME17 localization were explored in a co-transformation experiment. A new version of *Pro-PME17* tagged with *rfp,* under the control of *35S* promoter was prepared and transiently co-expressed with *SBT3.3-YFP* in the epidermal cells of tobacco leaves. The Pro-PME17 and SBT3.3 co-localize at the CW, and this is favoured over time as revealed by colocalization parameters (Figure 9). All these results strongly support the hypothesis that Pro-PME17 is released in the CW in an unprocessed and inactive form where, later when required, is activated by SBT3.3 to trigger immunity.

DISCUSSION

Plants exploit a great and local increase of PME activity in response to pathogens with different lifestyles (Bethke et al., 2014; Lionetti et al., 2014; Lionetti, 2015; Lionetti et al., 2017). *A. thaliana* induces the expression of specific PME isoforms during the attack of different pathogens. Among them, *Pro-PME17* is induced after the infection of a wide range of plant pathogens and can be considered a general biomarker of pathogenesis (Lionetti et al., 2012). *Botrytis cinerea* is an important fungal plant necrotrophic pathogen, that kills plant tissue prior to feeding using a range of toxic molecules to destroy host cells (Williamson et al., 2007; Dean et al., 2012). Pro-PME17 was recently involved in triggering PME activity and in resistance against *B. cinerea* (Del Corpo et al., 2020). The Pro region acts as an intramolecular inhibitor of Pro-PME17 activity. Here, intriguingly we note that all the PME isoforms induced in *A. thaliana* during *B. cinerea* infection are organized as zymogens in which the catalytic region is preceded by an N-terminal Pro region. The structural similarity revealed between the amino acid sequences of the Pro regions of these PMEs and the independent immunity-related PMEIs (AtPMEI10 and AtPMEI11) (Lionetti et al., 2017; Del Corpo et al., 2020) support their possible role as intramolecular inhibitors of the specific PMEs in each specific Pro-PME cluster. We therefore attempted to identify which possible proteases could be involved in the activation of PME activity against microbes. Different SBTs were associated to the processing of PMEs in plant physiology (Schaller et al., 2018). Most SBTs are targeted to the CW, where they contribute to the control of CW properties during growth and development. The *Arabidopsis* SBT3.5 was previously found to process Pro-PME17 releasing PME activity during root growth in *Arabidopsis* seedlings (Senechal et al., 2014a). SBT1.7 modulates PME activity in the mucilage release from *Arabidopsis* seed coats (Rautengarten et al., 2008). AtSBT6.1 is likely to be involved in maturation of a pectin methylesterase (Wolf et al., 2009). The evidence that the precursors of bZIP transcription factors,

RALF23 and GOLVEN1 are further substrates of AtSBT6.1 and that most SBTs are synthesized as inactive precursors could suggest that SBTs isoform could be part of an activation cascade, similar to that observed for caspases during plant programmed cell death events in mammals (Vartapetian et al., 2011; Paulus and Van der Hoorn, 2019).

Although SBTs were also associated to plant immunity their molecular substrates and their function remains largely unknowns (Figueiredo et al., 2014; Schaller et al., 2018; Godson and van der Hoorn, 2021). The tomato subtilisin-like protease SlSBT3 contributes to insect resistance in tomato. Although SlSBT3 was found to affect PME activity and the level of pectin methylesterification, these effects were unrelated to its role in herbivore defense (Meyer et al., 2016). Also, AtSBT5.2 and AtSBT3.14 were involved in different plant-pathogen interactions but their functions appear unrelated to PME activity (Lozano-Torres et al., 2014; Serrano et al., 2016). Here, we explored on the possible role of SBTs as post-transcriptional regulators of PME activity in *Arabidopsis* immunity against the necrotrophic fungus *B. cinerea*. Exploiting publicly available microarray data, we selected two genes, *SBT3.3* and *SBT3.5* co-expressed with *Pro-PME17* in *Arabidopsis* during *Botrytis* infection. SBT3.3 was previously discovered as a extracellular subtilase involved in the activation of *Arabidopsis* immunity against *Pseudomonas syringae* and *Hyaloperonospora arabidopsidis* (Ramirez et al., 2013) although its substrate remained unknown. Here, we demonstrated that *SBT3.3* and *SBT3.5* are induced in *Arabidopsis* leaves challenged with *Botrytis*. *SBT3.3* exhibited a higher fold-induction respect to SBT3.5. Interestingly, the expression of both *SBT* genes is also triggered in *Arabidopsis* against several pathogens. Moreover, *SBT3.3* and *SBT3.5* are induced by different bacterial and fungal elicitors of plant defense responses. SBT3.3 is specifically dedicated to plant defense because it is induced only during the infection process. However previous evidence indicates that SBT3.3 expression respond very rapidly to H_2O_2 and it enhances the activation of mitogen-activated protein kinases (MAPKs) following microbial attack (Ramirez et al., 2013). We detected SBT3.3 as a component of OGs signaling. All these evidence points to the involvement of SBT3.5 and, particularly of SBT3.3, as contributors in the activation of the earliest signaling events of PTI against *Botrytis* and several other pathogens.

The possible role of SBT3.3 and SBT3.5 as PME activators in *Arabidopsis* immunity against *B. cinerea* infection was explored. *sbt3.3-1*, *sbt3.3-2*, *sbt3.5-1*, *sbt3.5-2* mutants showed a significant higher susceptibility to the fungus when compared with WT. The significant lower induction of PME activity observed in *B. cinerea*-infected *sbt3.3* and *sbt3.5* mutants respect to WT plants indicates that

SBT3.3 and SBT3.5 are involved in the release of mature active PMEs to contrast the microbial invasion. The susceptibility- and PME-related effects are more marked in the *sbt3.3* mutant respect to *sbt3.5* mutants suggesting that SBT3.3 can have a major contribution on the total PME activity expressed in *Arabidopsis* against the fungus. This also suggests that the two SBTs analyzed in this study can target different Pro-PME isoforms. The involvement of multiple SBT-Pro-PME pairs is also suggested by the observed variability in the processing motifs of all the PME isoforms involved in *Arabidopsis-Botrytis* interaction. We revealed a significant higher induction of PME activity and a higher resistance to *Botrytis* in infected *SBT3.3-OE1* and *SBT3.3-OE2* leaves respect to untransformed plants. Overall, our evidence indicates that SBT3.3 and SBT3.5, by processing different Pro-PME isoforms, contribute to trigger PME activity to contrast *B. cinerea* infection. The absence of growth abnormalities and alteration of monosaccharide composition in the *sbt* mutants and SBT3.3OE lines indicate that these SBTs are mostly involved in plant immunity processes in leaves of adult plants.

The low level of CW methylesters detected in SBT3.3OE lines indicate that SBTs, by timely activating PMEs early at the point of fungal penetration, can favor the increase of charged carboxyl groups forming a higher amount of Ca^{2+}-mediated pectin crosslinks to reinforce the CW structure and the resistance to the microbe. Moreover, the SBT3.3-related pectin structural reinforcement is also accompanied by the stimulation of an immune response signaling. The higher induction of *WRKY33*, *PAD3*, *CYP81F2* and *WAK2* genes detected in *SBT3.3-OE1* plants respect to WT plants identifies a more robust immune response as mechanism contributing to the improved resistance observed in the transgenic plants. The induction of *WRKY33*, *PAD3* and *CYP81F2* by *SBT3.3* overexpression suggests the involvement of Camalexin and indole Glucosinolate accumulation. The evidence that WAK2 is highly expressed in transgenic plants suggest also the improvement of cell wall surveillance (Kohorn et al., 2014). Interestingly, WAK2 was demonstrated to require PME-mediated pectin de-methylesterification to activate OGs-dependent stress responses. We can hypothesize that SBT3.3 activates PME activity to favour WAK2 binding, and WAK2-OGs mediated stress signalling. Considering that OGs induce the expression of *SBT3.3*, *WRKY33*, *PAD3* and *CYP81F2* and that a *SBT3.3* self-activation was previously reported (Denoux et al., 2008; Ramirez et al., 2013), a positive feedback loop circuit based on PME activity, could be mounted to strengthen the activation of OGs-mediated defense responses. In addition, SBTs-dependent PME activity could also favour the binding and the functions of other PRR, like WAK1 and FERONIA, known to preferentially bind de-methylesterified crosslinked pectins (Decreux and Messiaen, 2005; Feng et al., 2018; Guo et al., 2018; Lin et al., 2018). Future efforts will be needed to explore on these hypotheses. All these observations

indicate SBTs and PME activities exploit a cooperation between CW integrity maintenance and PTI signalling to regulate defense responses after a CW damage (Engelsdorf et al., 2018). Although the specific pairs of SBT3.3, SBT3.5 and Pro-PMEs involved in plant immunity remain to be identified, we found that Pro-PME17 and SBT3.3 are both delivered in the apoplast using a conventional secretion pathway. Pro-PME17 reaches the cell wall before SBTs and their colocalization in the apoplast increase over time. This temporal separation could avoid a premature PME activation and pectin de-methylesterification in the secretory compartments. Later in the apoplast, plants can accumulate Pro-PMEs clusters as soluble and inactive receptors. At the right time, SBTs could be delivered in an apoplast already enriched in the inactive Pro-PMEs to rapidly derepress the inhibitory activity exerted by the Pro region. This mechanism could lead to a faster induction of PME activity at the point of pathogen penetration to amplify the early immune signalling underlying the defense response. In a similar mechanism, known as ectodomain shedding, the proteolytic cleavage of extracellular domains of cell surface proteins resulting in the activation of a variety of normal and pathological signalling processes in animals including growth factor signalling, cell adhesion, inflammation and cell survival (Lichtenthaler et al., 2018). This proposed SBTs function would be also in line with the negative regulation that speeds the response times of hormonal transcription networks in plants (Rosenfeld et al., 2002). The speed of a response, particularly to biotic stress, can be crucial for the survival of the sessile plant. Interestingly, SBT3.3 was involved in the physiological state called "priming", a sensory status able to induce a resistance faster and stronger respect to the same stimulus received before (Ramirez et al., 2013). It was previously hypothesized that priming could involve the accumulation of inactive proteins that becomes operative to initiate a signal amplification leading to a faster and stronger activation of defense responses (Bruce et al., 2007; Conrath, 2011; Ramirez et al., 2013). The processing of Pro-PMEs by SBT3.3 at a precise time and in the correct subcellular compartment could be part of the immune priming processes. Two PME-related DAMPs, OGs and MeOH are known to trigger defensive priming in plant immunity (Dorokhov et al., 2012; Komarova et al., 2014; Gamir et al., 2021; Giovannoni et al., 2021). The possibility that SBTs, trigger PMEs to assist and reinforce the OGs and MeOH signalling in priming is an interesting hypothesis to be investigated.

In conclusion, this study brings new insights into the molecular mechanisms underlying the activation of PME related immunity against necrotrophs increasing our understanding of the complexity of the interactions between plants and microbes. A switch on mechanism, mediated by SBTs for fine tuning PME activity and pectin integrity signaling, emerges providing knowledge about how plants modulate immunity. We identify Pro-PMEs as the target substrate processed by SBT3.3 indicating how this host

factor mediates immune prime activation. Future studies will be useful to identify the specific SBT-Pro-PME pairs and to quantify the contribution of PME activity to priming. Activation of Pro-PMEs and plant immunity by Subtilases processing becomes an effective genomic tool to engineer durable, broad-spectrum plant disease resistance and to avoid a growth-defense trade-offs.

Materials And Methods

Plant, Bacteria and Fungus growth conditions

Arabidopsis thaliana Wild-type Columbia (Col-0), *sbt* mutants and SBT3.3-OE seedlings were grown in solid MS/2 medium [Murashige and Skoog Medium including vitamins (2.2 g L^{-1}), 1% sucrose, 0.8% plant agar, pH 5.7] in a controlled environmental chamber maintained at 22°C and 70% relative humidity, with a 16h/8h day/night cycle (PAR level of 100 µmol $m^{-2}s^{-1}$). Adult plants were transferred on soil in a growth chamber at 22°C and 70% relative humidity under a 12 h/12h day/night cycle (PAR level of 120 µmol $m^{-2}s^{-1}$). *Sbt* mutants used include SALK_086092 (At1g32960; *sbt3.3-1*), SALK_107460 (At1g32960; *sbt3.3-2*), SAIL_400_F09 (At1g32940; *sbt3.5-1*) and GABI_672C08 (At1g32940; *sbt3.5-2*). All mutants are in Col-0 background and are T-DNA insertion lines obtained from the Nottingham *Arabidopsis* Stock Centre (NASC). *Nicotiana tabacum cv* SR1 seeds were sterilized using commercial grade bleach solution in the presence of 0.1% (v/v) for 15 min at room temperature and then washed three times for 5 min with distilled water before sowing. The seeds were germinated in a growth room at 25°C and 30% relative humidity under a 16h/8h day/night cycle (photosynthetic photon flux of 50 µmol $m^{-2}s^{-1}$). Three- to four-week-old plants from MS medium were transferred on soil and grown in a controlled-environment at 25°C and 40% relative humidity under a 16h/8h day/night cycle (photosynthetic photon flux of 120 µmol $m^{-2}s^{-1}$). *Escherichia coli* TOP10 cells was grown in LB agar plate (Luria-Bertani: tryptone 1%, yeast exctract 0.5%, NaCl 1%) containing ampicillin 50µg/ml and incubated overnight at 37°C. *Agrobacterium tumefaciens* (Strain GV3110) was grown in LB medium (Luria-Bertani: tryptone 1%, yeast exctract 0.5%, NaCl 1%) containing appropriate antibiotics (Rifampycin 100µg/ml and Spectomycin 100µg/ml or Kanamycin 50µg/ml) and incubated for 2 days at 28°C. *Botrytis cinerea* strain SF1 (Lionetti et al., 2007) was grown for 20 days on Malt Extract Agar at 20 g L^{-1} with Mycological Peptone at 10 g L^{-1} (MEP) at 23°C and 70% relative humidity in the dark before conidia collection.

For seed germination analysis, *A. thaliana* WT, sbt mutants and SBT3.3-OE seeds were washed in 2 mL of isopropanol for 30 seconds followed by washing in 2 mL of sterile water for 3 min in slow agitation. Seeds were treated with 2 mL of sterilization solution (400 µl NaClO, 1.6 ml sterile water)

for 5 min in slow agitation, followed by 4 washing steps in 2 ml of sterile water. For seed germination assay, triplicate sets of 60–70 sterilized seeds for each genotype were sown in Petri dishes on solid MS/2 medium in a controlled environmental chamber maintained at 22°C and 70% relative humidity, with a 16h/8h day/night cycle (PAR level of 100 µmol m-2s-1). Seeds germination rate, as the number of germinated seeds divided by the total amount of total seeds, were scored at 24, 48 and 72 hours.

Genotyping of T-DNA insertion mutants

Genomic DNA was extracted using RBC Bioscience Genomic DNA Extraction Kits, according to the manufacturer's instructions, from leaves of 4-week-old *Arabidopsis* wild-type and mutant plants and subjected to a PCR-based screening using sequences of primer, described in Supplemental Table S1, generated with Primer3 (https://primer3.ut.ee/). Taq Kapa DNA Polymerase (Kapa Biosystem) was used at 1 units/30 µl of assay. Amplification was carried out in presence of dNTPs (0.2 mM), 2.5 mM $MgCl_2$ and specific primers (10 µM) in the 1x buffer provide by the supplier. Conditions for amplification were: 95°C for 3 minutes; 36 cycles of amplification: 95°C for 30 sec, 60°C for 30 sec, 72°C for 60 sec, and a final extension of 72°C for 1 min. PCR products were separated by agarose gel electrophoresis and visualized by ethidium bromide staining. Plants homozygous for the mutations were propagated and used for all subsequent experiments.

Stable transformation of SBT3.3-OE *Arabidopsis* plants

Flowering *Arabidopsis* plants were transformed by floral dipping for 15 seconds in 200 mL of the culture medium with the inoculum of *Agrobacterium tumefaciens* C58 carrying the construction of interest. The plants were subsequently covered for 1 day to promote the infection. The culture medium for immersion was composed of MS 2.2 g/L and sucrose 5% (p/v), supplemented with Silwet 0.005% and BAP 0.05 ug/mL. Subsequently, the selection of homozygous transgenic plants for the *SBT3.3-YFP* construction was carried out by means of selection with BASTA herbicide.

Elicitor Treatment and Gene expression analysis

B. cinerea-infected or Mock-inoculated leaves were frozen in liquid nitrogen and homogenized using the mixer mill MM301 (RETSCH) and using inox beads (5 mm diameter) for about 1 min at 30 Hz, and total RNA was extracted with Isol-RNA Lysis Reagent (5′-Prime) according to the manufacturer's instructions. RNA was treated with RQ1 DNase (Promega), and first-strand complementary DNA (cDNA) was synthesized using ImProm-II reverse transcriptase (Promega). Quantitative Reverse

Transcription PCR analysis was performed using a CFX96 Real-Time System (Bio-Rad). One microliter of cDNA (corresponding to 50 ng of total RNA) was amplified in 20 µL of reaction mix containing 1× Go Taq qPCR Master Mix (Promega) and 0.5 µM of each primer described in Supplemental Table S2. Conditions for amplification were: 95°C for 2 minutes; 46 cycles of amplification: 95°C for 15 sec, 58°C for 15 sec, and a final extension of 72°C for 15 sec. Expression levels of each gene, relative to the UBIQUITIN5 (UBQ5) gene, were determined using a modification of the Pfaffl method (Pfaffl, 2001). Primer sequences were generated with Primer3 software (https://primer3.ut.ee/). Seedlings of 10-days-old *Arabidopsis* cultured in liquid MS/2 medium were treated for 1h with OG_S (40 µg mL^{-1}) or water as a control, collected and processed for RNA extraction as described above.

Arabidopsis thaliana* infection with *Botrytis cinerea

Conidia of *B. cinerea* were harvested by washing the surface of the mycelium with sterile distilled water. Conidia suspensions were filtered to remove residual mycelium and the conidia concentration was determined using a Thoma chamber. Fully developed leaves from 4-week-old *A. thaliana* plants were infected with $1x10^6$ conidia mL^{-1} incubated in Potato Dextrose Broth (PDB) at 24 g L^{-1}. Six droplets of spore suspension (5 µL each) were placed on the surface of each leaf. Mock-inoculation was performed using PDB. Plants were incubated at 24°C with a 12h/12h day/night photoperiod. The lesion size produced by *B. cinerea* was evaluated as an indicator of susceptibility to the fungus.

Determination of PME activity, fungal diffusion and H_2O_2 accumulation

Total protein extracts were obtained by homogenizing uninfected and infected *Arabidopsis* leaves in the presence of 1M NaCl, 12.5 mM Citric Acid, 50 mM Na_2HPO_4, 0.02 % Sodium Azide, protease inhibitor 1:200 v/v (P8849, Sigma), pH 6.5. Each sample was resuspended in 500 µL of protein Extraction Buffer. The homogenates were shaken for 3 h at 4°C, centrifuged at 13.000 x g for 15 min, and the supernatant (400 µL) collected. Protein concentration was determined in the supernatants using Bradford protein assay method (Bradford reagent, Sigma–Aldrich), a standard curve was performed using BSA (bovin serum albumine) at 1 mg mL^{-1}. PME activity was evaluated by using PECTOPLATE assay (Lionetti, 2015): PECTOPLATE was prepared with 0.1% (w/v) of apple pectin (molecular weight range 30,000–100,000 Da; 70–75% esterification; 76282, Sigma-Aldrich, St. Louis), 1% (w/v) SeaKem® LE agarose (Lonza, Basel, Switzerland, Catalog no: 50004E), 12.5 mM citric acid and 50 mM Na_2HPO_4, pH 6.5. Equal amounts of protein samples (2 µg of total protein in 20 µL) were

loaded in each well of PECTOPLATE. Plates were incubated at 30°C for 16 h, and stained with 0.05% (w/v) Ruthenium Red (RR) (R2751; Sigma-Aldrich, St. Louis) for 30 min. The plates were de-stained by several washes with water and the area of the fuchsia-stained haloes, resulting from de-methylesterification of pectin and the area of inner unstained haloes, resulting from the hydrolysis of pectin in the gel, were measured with ImageJ software (Abramoff, Magalhes, and am 2004). Known amounts of commercially available PME from orange (Citrus spp.) peel (P5400; Sigma-Aldrich) was used in the PECTOPLATE to generate a standard curve used to calculate PME activity in the protein extracts.

For the detection of *B. cinerea* hyphae, detached leaves were incubated for 30 min in lactophenol Trypan Blue solution (water: glycerol: lactic acid: phenol [1:1:1:1] + Trypan Blue solution [1 mg mL^{-1}; Sigma-Aldrich]). Thereafter, leaves were washed for overnight with gentle agitation in absolute ethanol to remove chlorophyll. Leaves were assayed for H_2O_2 accumulation employing 3,3′-diaminobenzidine staining as previously described (Daudi and O'Brien, 2012). Leaves were mounted in 50% glycerol and examined by light microscopy using Nikon eclipse E200 microscope. Images were taken with a Nikon Digital Sight DS-Fi1c camera

Determination of Monosaccharide Composition of CW and MEOH quantification

Extraction of alcohol-insoluble residue, CW monosaccharide composition and the determination of CW methylesters were performed as previously described (Lionetti et al., 2017).

SBT3.3-YFP and PME17-GFP/RFP Gene Constructs

For the SBT3.3-YFP overexpressing construct, a full-length cDNA for SBT3.3 was amplified by PCR using Pfu DNA polymerase (Stratagene, San Diego, CA) and specific primers, described in Supplemental Table S3, including Gateway adapters: BP SBT3.3 FW and BP SBT3.3 RV and recombined into pDONR207 using BP ClonaseMixII kit (Invitrogen). After sequencing, the construct was recombined with pB7FWG2 destination vector (YFP in C-terminal) using LR ClonaseMixII kit (Invitrogen) and introduced into *Arabidopsis* (*sbt3.3*) via Agrobacterium transformation.

For PME17-GFP/RFP overexpressing constructs, the full-length cDNA for PME17 was amplified by PCR using *TakaRa* Ex Taq DNA polymerase (TAKARA, Kyoto), and specific primers flanked by Gateway adapters, attB sequences, described in Supplemental Table S3. PCR amplified attB-flanked DNA was recombined into pDONR221 using BP ClonaseMixII kit (Invitrogen). Specific pDESTs, pK7FWG2 and pK7RWG2,0, were used for GFP and RFP fusion in C-terminus to obtain Pro-PME17-

GFP and Pro-PME17-RFP, respectively. All constructs were checked by sequencing (Eurofins Genomics, https://eurofinsgenomics.eu/). The Gateway constructs, PME17-GFP, PME17-RFP, SBT3.3-YFP, SBT3.3-mCherry, RFP-HDEL, ST52-mCherry, XTH11-RFP and pm-rk were introduced into *Agrobacterium tumefaciens* (Strain GV3110) and the agroinfiltration was performed in *Nicotiana tabacum* leaves as previously described (De Caroli et al., 2011).

Transient transformation of *Nicotiana tabacum* leaves and confocal Laser Scanning Microscopy

Almost fully expanded Nicotiana tabacum 6-week-old leaves were infiltrated with a suspension of Agrobacterium tumefaciens bearing the relevant construct in 2mM Na3PO4; 50mM 2-(N-morpholine)-ethanesulphonic acid (MES); glucose 0.5%; acetosyringone 100µM; pH= 5.6 at an OD_{600}=0.5. After 48 and 52 hours post infiltration (hpi) fluorescence was analyzed in infiltrated leaves by confocal microscopy. For co-infiltration, Agrobacterium cultures grown separately were adjusted to an OD_{600}=0.5 and mixed prior to infiltration. Transiently transformed tobacco leaves were observed using a confocal laser scanning microscope LSM710 Zeiss (http://www.zeiss.com) mounting material in water as previously described (De Caroli et al., 2011). GFP and YFP were detected within the short 505–530 nm wavelength range, assigning the green color; RFP and mCherry were detected within 560–615 nm, assigning the red color. Excitation wavelengths of 488 and 543 nm were used. The laser power was set to a minimum and appropriate controls were made to ensure there was no bleed-through from one channel to the other. Images were processed using PHOTOSHOP7.0 (Adobe, https://www.adobe.com). For quantitative colocalization analyses, the overlap coefficient (OC, after Manders) and the Pearson's correlation coefficient (R) were evaluated as previously reported (De Caroli et al., 2011).

Bioinformatics tools

The Expression Angler tool of the Bio-Analytic Resource for Plant Biology (BAR, http://bar.utoronto.ca/welcome.htm) was used for co-expression analysis. E-plant (https://bar.utoronto.ca/eplant/) was used for to study developmental map and biotic stresses. Chromas was used to manage both nucleotide sequences and amino acids (https://chromas.software.informer.com/2.5/). Primer3 (https://primer3.ut.ee/) was used to design primers respectively for Gene expression analysis and Genotyping analysis. ImageJ was used to calculate the area of the haloes in PECTOPLATE assay (http://imagej.nih.gov/ij/download.html). DNAMAN software (Lynnon, BioSoft, Quebec, Canada, https://www.lynnon.com/) was used for

amino acid sequence analyses. Genevestigator Meta-Analyzer Tools (www.genevestigator.ethz.ch/at/) was used to analyze *SBT3.3* and *SBT3.5* gene expression during infection of *Arabidopsis* with different pathogens and DAMPs and PAMPs treatments.

Quantification and statistical analysis

The statistical significance of the difference in gene expression between specific samples was analyzed through ANOVA followed by Tukey's test ($P < 0.05$), for all other statistical analyses the Student's t-test was used. The error bars represent standard deviation of mean.

Accession numbers

The genes used in this study have the following accession numbers: SBT3.3, At1g32960; SBT3.5, At1g32940; UBQ5, At3g62250; PAD3, At3g26830; CYP81F2, At5g57220; PME17, At2g45220; PMEI10, At1g62760; WAK2, At1G21270; At2g38470, WRKY33. *B. cinerea* β-tubulin, MG949129.1.

Supplemental data

Supplemental Figure S1. Gene structure and alignment of amino acid sequences of Pro-PMEs induced in Arabidopsis during *B. cinerea* infection.

Supplemental Figure S2. *SBT3.3* and *SBT3.5* gene expression in *Arabidopsis* challenged with *Botrytis cinerea*.

Supplemental Figure S3. *SBT3.3* and *SBT3.5* gene expression during infection of *Arabidopsis* with different pathogens and after different DAMPs and PAMPs treatments

Supplemental Figure S4. Seed morphology and germination are not altered in *sbt3.3*, *sbt3.5* mutants and *SBT3.3*-OE lines.

Supplemental Figure S5. Arabidopsis *sbt3.3-1*, *sbt3.5-1* mutants and SBT3.3-OE1 line are not defective in H_2O_2 accumulation against *Botrytis*.

Supplemental Table S1. Primers used for genotyping

Supplemental Table S2. Primers used for qRT-PCR

Supplemental Table S3. Primers used to obtain Pro-PME17 and SBT3.3 fluorescent constructs with Gateway system.

Acknowledgments

We thank Marco Greco for technical assistance.

Funding

The work was supported by Sapienza University of Rome, Grants RM120172B78CFDF2, RM11916B7A142CF1 and RG12117A898EABE0 to VL and AR12117A8A4A1ADC to DC and LV.

Author contributions

V.L. conceived the research; G.P, P.V and L.V. developed the experimental designs and supervised the experiments; D.C., D.D.C, M.O.M and M.D.C performed the experiments; D.C., M.D.C, G.P, P.V. and V.L. analysed data; All authors contributed to discussing the results of this manuscript. V.L. wrote the article with contributions of all the authors

REFERENCES

Abramoff MD, Magalhães PJ, am SJ (2004) Image processing with ImageJ. Biophotonics international **11**: 36–42

AbuQamar S, Moustafa K, Tran LS (2017) Mechanisms and strategies of plant defense against Botrytis cinerea. Critical Reviews in Biotechnology **37**: 262–274

An SH, Sohn KH, Choi HW, Hwang IS, Lee SC, Hwang BK (2008) Pepper pectin methylesterase inhibitor protein CaPMEI1 is required for antifungal activity, basal disease resistance and abiotic stress tolerance. Planta **228**: 61–78

Bethke G, Grundman RE, Sreekanta S, Truman W, Katagiri F, Glazebrook J (2014) Arabidopsis PECTIN METHYLESTERASES Contribute to Immunity Against Pseudomonas syringae. Plant Physiol **164**: 1093–1107

Birkenbihl RP, Diezel C, Somssich IE (2012) Arabidopsis WRKY33 is a key transcriptional regulator of hormonal and metabolic responses toward Botrytis cinerea infection. Plant Physiol **159**: 266–285

Bosch M, Cheung AY, Hepler PK (2005) Pectin Methylesterase, a Regulator of Pollen Tube Growth. Plant Physiol **138**: 1334–1346

Bruce TJA, Matthes MC, Napier JA, Pickett JA (2007) Stressful “memories” of plants: Evidence and possible mechanisms. Plant Science **173**: 603–608

Brutus A, Sicilia F, Macone A, Cervone F, De Lorenzo G (2010) A domain swap approach reveals a role of the plant wall-associated kinase 1 (WAK1) as a receptor of oligogalacturonides. Proc Natl Acad Sci USA **107**: 9452–9457

Clay NK, Adio AM, Denoux C, Jander G, Ausubel FM (2009) Glucosinolate metabolites required for an Arabidopsis innate immune response. Science **323**: 95–101

Coculo D, Lionetti V (2022) The Plant Invertase/Pectin Methylesterase Inhibitor Superfamily. Frontiers in Plant Science **13**: 863892

Conrath U (2011) Molecular aspects of defence priming. Trends in Plant Science **16**: 524–531

Daudi A, O’Brien JA (2012) Detection of Hydrogen Peroxide by DAB Staining in Arabidopsis Leaves. Bio Protoc **2**: e263

De Caroli M, Lenucci MS, Di Sansebastiano GP, Dalessandro G, De Lorenzo G, Piro G (2011) Protein trafficking to the cell wall occurs through mechanisms distinguishable from default sorting in tobacco. Plant J **65**: 295–308

De Caroli M, Lenucci MS, Manualdi F, Dalessandro G, De Lorenzo G, Piro G (2015) Molecular dissection of Phaseolus vulgaris polygalacturonase-inhibiting protein 2 reveals the presence of hold/release domains affecting protein trafficking toward the cell wall. Front.Plant Sci. 6:

646 **De Caroli M, Manno E, Piro G, Lenucci MS** (2021) Ride to cell wall: Arabidopsis XTH11, XTH29 and XTH33
647 exhibit different secretion pathways and responses to heat and drought stress. The Plant Journal **107**:
648 448–466

649 **Dean R, van Kan JAL, Pretorius ZA, Hammond-Kosack KE, Di Pietro A, Spanu PD, Rudd JJ, Dickman M,**
650 **Kahmann R, Ellis J, et al** (2012) The Top 10 fungal pathogens in molecular plant pathology. MolPlant
651 Pathol **13**: 414–430

652 **Decreux A, Messiaen J** (2005) Wall-associated kinase WAK1 interacts with cell wall pectins in a calcium-induced
653 conformation. Plant Cell Physiol **46**: 268–278

654 **Dedeurwaerder S, Menu-Bouaouiche L, Mareck A, Lerouge P, Guerineau F** (2008) Activity of an atypical
655 Arabidopsis thaliana pectin methylesterase. Planta **229**: 311–21

656 **Del Corpo D, Fullone MR, Miele R, Lafond M, Pontiggia D, Grisel S, Kieffer-Jaquinod S, Giardina T, Bellincampi**
657 **D, Lionetti V** (2020) AtPME17 is a functional Arabidopsis thaliana pectin methylesterase regulated by
658 its PRO region that triggers PME activity in the resistance to Botrytis cinerea. Molecular Plant Pathology
659 **21**: 1620–1633

660 **Denoux C, Galletti R, Mammarella N, Gopalan S, Werck D, De Lorenzo G, Ferrari S, Ausubel FM, Dewdney J**
661 (2008) Activation of defense response pathways by OGs and Flg22 elicitors in Arabidopsis seedlings.
662 Mol Plant **1**: 423–445

663 **Doehlemann G, Hemetsberger C** (2013) Apoplastic immunity and its suppression by filamentous plant
664 pathogens. New Phytologist **198**: 1001–1016

665 **Dorokhov YL, Komarova TV, Petrunia IV, Frolova OY, Pozdyshev DV, Gleba YY** (2012) Airborne Signals from a
666 Wounded Leaf Facilitate Viral Spreading and Induce Antibacterial Resistance in Neighboring Plants. Plos
667 Pathogens 8:

668 **Engelsdorf T, Gigli-Bisceglia N, Veerabagu M, McKenna JF, Vaahtera L, Augstein F, Does DV der, Zipfel C,**
669 **Hamann T** (2018) The plant cell wall integrity maintenance and immune signaling systems cooperate to
670 control stress responses in Arabidopsis thaliana. Sci Signal **11**: eaao3070

671 **Feng W, Kita D, Peaucelle A, Cartwright HN, Doan V, Duan Q, Liu M-C, Maman J, Steinhorst L, Schmitz-Thom**
672 **I, et al** (2018) The FERONIA Receptor Kinase Maintains Cell-Wall Integrity during Salt Stress through
673 Ca2+ Signaling. Curr Biol **28**: 666-675.e5

674 **Ferrari S, Savatin DV, Sicilia F, Gramegna G, Cervone F, De Lorenzo G** (2013) Oligogalacturonides: plant
675 damage-associated molecular patterns and regulators of growth and development. Front.Plant Sci. doi:
676 10.3389/fpls.2013.00049:

677 **Figueiredo A, Monteiro F, Sebastiana M** (2014) Subtilisin-like proteases in plant-pathogen recognition and
678 immune priming: a perspective. FrontPlant Sci **5**: 739.

679 **Figueiredo J, Sousa Silva M, Figueiredo A** (2018) Subtilisin-like proteases in plant defence: the past, the
680 present and beyond: Subtilases in plant defence. Molecular Plant Pathology **19**: 1017–1028

681 **Gamir J, Minchev Z, Berrio E, García JM, De Lorenzo G, Pozo MJ** (2021) Roots drive oligogalacturonide-induced
682 systemic immunity in tomato. Plant, Cell & Environment **44**: 275–289

683 **Giovannoni M, Lironi D, Marti L, Paparella C, Vecchi V, Gust AA, De Lorenzo G, Nürnberger T, Ferrari S** (2021)
684 The Arabidopsis thaliana LysM-containing Receptor-Like Kinase 2 is required for elicitor-induced
685 resistance to pathogens. Plant, Cell & Environment **44**: 3775–3792

686 **Godson A, van der Hoorn RAL** (2021) The front line of defence: a meta-analysis of apoplastic proteases in plant
687 immunity. Journal of Experimental Botany **72**: 3381–3394

688 **Guo H, Nolan TM, Song G, Liu S, Xie Z, Chen J, Schnable PS, Walley JW, Yin Y** (2018) FERONIA Receptor Kinase
689 Contributes to Plant Immunity by Suppressing Jasmonic Acid Signaling in Arabidopsis thaliana. Curr Biol
690 **28**: 3316-3324.e6

691 **Ha CM, Rao X, Saxena G, Dixon RA** (2021) Growth–defense trade-offs and yield loss in plants with engineered
692 cell walls. New Phytologist **231**: 60–74

693 **Hann CT, Bequette CJ, Dombrowski JE, Stratmann JW** (2014) Methanol and ethanol modulate responses to
694 danger- and microbe-associated molecular patterns. Front.Plant Sci. 5:

695 **He Z, Webster S, He SY** (2022) Growth-defense trade-offs in plants. Curr Biol **32**: R634–R639

696 **Hou S, Jamieson P, He P** (2018) The cloak, dagger, and shield: proteases in plant–pathogen interactions.
697 Biochemical Journal **475**: 2491–2509

698 **Huot B, Yao J, Montgomery BL, He SY** (2014) Growth–Defense Tradeoffs in Plants: A Balancing Act to Optimize
699 Fitness. Molecular Plant **7**: 1267–1287

700 **Khan AR, James MN** (1998) Molecular mechanisms for the conversion of zymogens to active proteolytic
701 enzymes. Protein Sci **7**: 815–836

702 **Kohorn BD, Kohorn SL** (2012) The cell wall-associated kinases, WAKs, as pectin receptors. FrontPlant Sci **3**: 88

703 **Kohorn BD, Kohorn SL, Saba NJ, Martinez VM** (2014) Requirement for Pectin Methyl Esterase and Preference
704 for Fragmented over Native Pectins for Wall-associated Kinase-activated, EDS1/PAD4-dependent Stress
705 Response in Arabidopsis. JBiolChem **289**: 18978–18986

706 **Komarova TV, Sheshukova EV, Dorokhov YL** (2014) Cell wall methanol as a signal in plant immunity.
707 Front.Plant Sci. 5:

708 **Lichtenthaler SF, Lemberg MK, Fluhrer R** (2018) Proteolytic ectodomain shedding of membrane proteins in
709 mammals—hardware, concepts, and recent developments. EMBO J **37**: e99456

710 **Lin W, Tang W, Anderson CT, Yang Z** (2018) FERONIA's sensing of cell wall pectin activates ROP GTPase
711 signaling in Arabidopsis. bioRxiv 269647

712 **Lin W, Tang W, Pan X, Huang A, Gao X, Anderson CT, Yang Z** (2021) Arabidopsis pavement cell morphogenesis
713 requires FERONIA binding to pectin for activation of ROP GTPase signaling. Current Biology
714 S096098222101589X

715 **Lionetti V** (2015) PECTOPLATE: the simultaneous phenotyping of pectin methylesterases, pectinases, and
716 oligogalacturonides in plants during biotic stresses. FrontPlant Sci **6**: 1–8

717 **Lionetti V, Cervone F, Bellincampi D** (2012) Methyl esterification of pectin plays a role during plant-pathogen
718 interactions and affects plant resistance to diseases. JPlant Physiol **169**: 1623–1630

719 **Lionetti V, Fabri E, De Caroli M, Hansen AR, Willats WG, Piro G, Bellincampi D** (2017) Three pectin methyl
720 esterase inhibitors protect cell wall integrity for immunity to Botrytis. Plant Physiol **Jan 12.**: pii:
721 pp.01185.2016.

722 **Lionetti V, Francocci F, Ferrari S, Volpi C, Bellincampi D, Galletti R, D'Ovidio R, De Lorenzo G, Cervone F** (2010)
723 Engineering the cell wall by reducing de-methyl-esterified homogalacturonan improves saccharification
724 of plant tissues for bioconversion. Proc Natl Acad Sci USA **107**: 616–621

725 **Lionetti V, Raiola A, Camardella L, Giovane A, Obel N, Pauly M, Favaron F, Cervone F, Bellincampi D** (2007)
726 Overexpression of Pectin Methylesterase Inhibitors in Arabidopsis Restricts Fungal Infection by Botrytis
727 cinerea. Plant Physiol **143**: 1871–1880

728 **Lionetti V, Raiola A, Cervone F, Bellincampi D** (2014) Transgenic expression of pectin methylesterase inhibitors
729 limits tobamovirus spread in tobacco and Arabidopsis. MolPlant Pathol **15**: 265–274

730 **Liu N, Sun Y, Pei Y, Zhang X, Wang P, Li X, Li F, Hou Y** (2018) A Pectin Methylesterase Inhibitor Enhances
731 Resistance to Verticillium Wilt1[OPEN]. Plant Physiol **176**: 2202–2220

732 **Lozano-Torres JL, Wilbers RHP, Warmerdam S, Finkers-Tomczak A, Diaz-Granados A, Schaik CC van, Helder J,**
733 **Bakker J, Goverse A, Schots A, et al** (2014) Apoplastic Venom Allergen-like Proteins of Cyst Nematodes
734 Modulate the Activation of Basal Plant Innate Immunity by Cell Surface Receptors. PLOS Pathogens **10**:
735 e1004569

736 **Meyer M, Huttenlocher F, Cedzich A, Procopio S, Stroeder J, Pau-Roblot C, Lequart-Pillon M, Pelloux J, Stintzi**
737 **A, Schaller A** (2016) The subtilisin-like protease SBT3 contributes to insect resistance in tomato. EXBOTJ
738 **67**: 4325–4338

739 **Nelson BK, Cai X, Nebenfuhr A** (2007) A multicolored set of in vivo organelle markers for co-localization studies
740 in Arabidopsis and other plants. Plant J **51**: 1126–1136

741 **Ogawa S, Wakatake T, Spallek T, Ishida JK, Sano R, Kurata T, Demura T, Yoshida S, Ichihashi Y, Schaller A, et al**
742 (2021) Subtilase activity in intrusive cells mediates haustorium maturation in parasitic plants. Plant
743 Physiology **185**: 1381–1394

744 **Osorio S, Bombarely A, Giavalisco P, Usadel B, Stephens C, Araguez I, Medina-Escobar N, Botella MA, Fernie**
745 **AR, Valpuesta V** (2011) Demethylation of oligogalacturonides by FaPE1 in the fruits of the wild
746 strawberry Fragaria vesca triggers metabolic and transcriptional changes associated with defence and
747 development of the fruit. JExpBot **62**: 2855–2873

748 **Osorio S, Castillejo C, Quesada MA, Medina-Escobar N, Brownsey GJ, Suau R, Heredia A, Botella MA,**
749 **Valpuesta V** (2008) Partial demethylation of oligogalacturonides by pectin methyl esterase 1 is
750 required for eliciting defence responses in wild strawberry (Fragaria vesca). Plant J **54**: 43–55

751 **Paulus JK, Van der Hoorn RAL** (2019) Do proteolytic cascades exist in plants? Journal of Experimental Botany
752 **70**: 1997–2002

753 **Pelloux J, Rustérucci C, Mellerowicz EJ** (2007) New insights into pectin methylesterase structure and function.
754 Trends Plant Sci **12**: 267–277

755 **Pogorelko G, Lionetti V, Fursova O, Sundaram RM, Qi MS, Whitham SA, Bogdanove AJ, Bellincampi D,**
756 **Zabotina OA** (2013) Arabidopsis and Brachypodium distachyon Transgenic Plants Expressing Aspergillus
757 nidulans Acetylesterases Have Decreased Degree of Polysaccharide Acetylation and Increased
758 Resistance to Pathogens. Plant Physiol **162**: 9–23

759 **Ramirez V, Lopez A, Mauch-Mani B, Gil MJ, Vera P** (2013) An Extracellular Subtilase Switch for Immune
760 Priming in Arabidopsis. Plos Pathogens 9:

761 **Rautengarten C, Steinhauser D, Bussis D, Stintzi A, Schaller A, Kopka J, Altmann T** (2005) Inferring Hypotheses
762 on Functional Relationships of Genes: Analysis of the Arabidopsis thaliana Subtilase Gene Family.
763 PLoS.Comput.Biol. 1:

764 **Rautengarten C, Usadel B, Neumetzler L, Hartmann J, Büssis D, Altmann T** (2008) A subtilisin-like serine
765 protease essential for mucilage release from Arabidopsis seed coats. The Plant Journal **54**: 466–480

766 **Reem N, Pogorelko G, Lionetti V, Chambers L, Held MA, Bellincampi D, Zabotina OA** (2016) Decreased
767 polysaccharide feruloylation compromises plant cell wall integrity and increases susceptibility to
768 necrotrophic fungal pathogens. FrontPlant Sci **7**: 630, doi: 10.3389/fpls.2016.00630

769 **Rosenfeld N, Elowitz MB, Alon U** (2002) Negative autoregulation speeds the response times of transcription
770 networks. J Mol Biol **323**: 785–793

771 **Schaller A** (2004) A cut above the rest: the regulatory function of plant proteases. Planta **220**: 183–197

772 **Schaller A, Stintzi A, Rivas S, Serrano I, Chichkova NV, Vartapetian AB, Martínez D, Guiamét JJ, Sueldo DJ, van**
773 **der Hoorn RAL, et al** (2018) From structure to function - a family portrait of plant subtilases. New
774 Phytol **218**: 901–915

775 **Senechal F, Graff L, Surcouf O, Marcelo P, Rayon C, Bouton S, Mareck A, Mouille G, Stintzi A, Hofte H, et al**
776 (2014a) Arabidopsis PECTIN METHYLESTERASE17 is co-expressed with and processed by SBT3.5, a
777 subtilisin-like serine protease. AnnBot **114**: 1161–1175

778 **Senechal F, Wattier C, Rusterucci C, Pelloux J** (2014b) Homogalacturonan-modifying enzymes: structure,
779 expression, and roles in plants. JExpBot **65**: 5125–5160

780 **Serrano I, Buscaill P, Audran C, Pouzet C, Jauneau A, Rivas S** (2016) A non canonical subtilase attenuates the
781 transcriptional activation of defence responses in Arabidopsis thaliana. eLife **5**: e19755

782 **Siegmund U, Viefhues A** (2016) Reactive Oxygen Species in the Botrytis – Host Interaction. *In* S Fillinger, Y Elad,
783 eds, Botrytis – the Fungus, the Pathogen and its Management in Agricultural Systems. Springer
784 International Publishing, Cham, pp 269–289

785 **Stegmann M, Monaghan J, Smakowska-Luzan E, Rovenich H, Lehner A, Holton N, Belkhadir Y, Zipfel C** (2017)
786 The receptor kinase FER is a RALF-regulated scaffold controlling plant immune signaling. Science **355**:
787 287–289

788 **Tornero P, Conejero V, Vera P** (1996) Primary structure and expression of a pathogen-induced protease (PR-
789 P69) in tomato plants: Similarity of functional domains to subtilisin-like endoproteases. Proceedings of
790 the National Academy of Sciences **93**: 6332–6337

791 **Vartapetian AB, Tuzhikov AI, Chichkova NV, Taliansky M, Wolpert TJ** (2011) A plant alternative to animal
792 caspases: subtilisin-like proteases. Cell Death Differ **18**: 1289–1297

793 **Wang S, Xing R, Wang Y, Shu H, Fu S, Huang J, Paulus JK, Schuster M, Saunders DGO, Win J, et al** (2021)
794 Cleavage of a pathogen apoplastic protein by plant subtilases activates host immunity. New Phytol **229**:
795 3424–3439

796 **Williamson B, Tudzynski B, Tudzynski P, Kan J a. LV** (2007) Botrytis cinerea: the cause of grey mould disease.
797 Molecular Plant Pathology **8**: 561–580

798 **Wolf S, Rausch T, Greiner S** (2009) The N-terminal pro region mediates retention of unprocessed type-I PME in
799 the Golgi apparatus. The Plant Journal **58**: 361–375

800 **Wormit A, Usadel B** (2018) The Multifaceted Role of Pectin Methylesterase Inhibitors (PMEIs). Int J Mol Sci.
801 doi: 10.3390/ijms19102878

802 **Zhou J-M, Zhang Y** (2020) Plant Immunity: Danger Perception and Signaling. Cell **181**: 978–989

803 **Zhou N, Tootle TL, Glazebrook J** (1999) Arabidopsis PAD3, a gene required for camalexin biosynthesis, encodes
804 a putative cytochrome P450 monooxygenase. Plant Cell **11**: 2419–28

805

806

807

Figure legends

Figure 1. *SBT3.3* and *SBT3.5* are induced in *Arabidopsis* during *B. cinerea* infection and SBT3.3 is induced by OGs treatment. A) *SBT3.3* and **B)** *SBT3.5* expression was analysed in *B. cinerea* infected or mock-inoculated leaves at the indicated hours post inoculation (hpi) by qPCR. M = Mock inoculated leaves. B = *B. cinerea* inoculated leaves. The expression of **C)** *SBT3.3* and **D)** *SBT3.5* was analysed in Arabidopsis WT seedlings after 1 hour of treatment with OGs or with water (H_2O) as a control. The expression levels were normalized to *Ubiquitin5* expression. Data represent mean ± SD (n=3). The experiments were repeated three times with similar results.

Figure 2. Isolation of Arabidopsis *SBT3.3* and *SBT3.5* T-DNA insertional mutants. A) Schematic representation of *SBT3.3* and *SBT3.5* gene structures. The localization of T-DNA insertions in the gene sequences are shown (black arrows). 5′-UTR and 3′-UTR are represented in grey, exons in white and introns as a black line. **B)** The expression of *SBT3.3* and *SBT3.5* was analyzed in the respective mutants and WT plants at 24-hour post inoculation with *B. cinerea*. The expression levels were normalized to *Ubiquitin 5* expression. The experiments were repeated three times with similar results. **C)** Representative pictures illustrating the morphology of vegetative rosettes (four-weeks old plants) of *sbt3.3* and *sbt3.5* mutants compared with WT. **D)** The monosaccharide composition of cell wall matrix polysaccharides was compared in leaves of *sbt3.3* and s*bt3.5* mutants and WT plants. The molar percentages of Fucose (Fuc), Rhamnose (Rha), Arabinose (Ara), Galactose (Gal), Glucose (Glu), Xylose (Xyl), Mannose (Man), Galacturonic Acid (Gal A) and Glucuronic Acid (Glc A) were quantified. The results represent the mean ± SD (n≥3). Monosaccharide datasets are not significantly different according to analysis of variance (ANOVA) followed by Tukey's test ($P < 0.05$).

Figure 3. SBT3.3 and SBT3.5 regulate PME activity during disease. A) Schematic representation of the binding of Ruthenium Red to de-methylesterified pectin. **B)** Leaves of Arabidopsis WT and of *sbt* mutants were inoculated with *Botrytis* and Mock and PME activity were quantified at 24-hour post inoculation (hpi). The results represent the mean ± SD (n = 6). The different letters on the bars indicate datasets significantly different according to ANOVA followed by Tukey's test ($P < 0.05$).

Figure 4. The lack of *SBT3.3 and SBT3.5* expression reduces *Arabidopsis* resistance to *Botrytis cinerea*. A) Quantification of lesion areas produced by the spreading of the fungus at 24 hours post

infections. Data represent mean ± SE (n ≥14 lesions for each genotype). Different letters indicate statistically significant differences, according to ANOVA followed by Tukey's significance test ($P < 0.05$). **B)** Photographs showing lesion areas produced by *Botrytis* on leaves of Arabidopsis WT, *sbt3.3-1 and sbt3.5-1* mutants (left) and microphotographs showing *Botrytis* colonization revealed by trypan blue staining (right). Bars = 1mm.

Figure 5. The *SBT3.3* overexpression in Arabidopsis does not alter rosette growth and cell wall composition. A) The expression of *SBT3.3* was analyzed in the *SBT3.3-OE1* and *SBT3.3-OE2* transgenic plants at 24-hour post inoculation with Mock and *B. cinerea* spores. The expression levels were normalized to *Ubiquitin5* expression. The experiments were repeated three times with similar results. **B)** Representative pictures illustrating the morphology of vegetative rosettes of *SBT3.3* overexpressing plants compared with WT plants. **C)** The molar percentages of Fucose (Fuc), Rhamnose (Rha), Arabinose (Ara), Galactose (Gal), Glucose (Glu), Xylose (Xyl), Mannose (Man), Galacturonic Acid (Gal A) and Glucuronic Acid (Glc A) were quantified. The results represent the mean ± SD (n ≥ 3). Monosaccharide datasets are not significantly different according to analysis of variance (ANOVA) followed by Tukey's test ($P < 0.05$).

Figure 6. The *SBT3.3* overexpression overactivates PME activity restricting *Botrytis* infection. A) Leaves of Arabidopsis WT and of *SBT3.3-OE* plants were inoculated with *Botrytis* and Mock and PME activity were quantified at 24-hour post inoculation. The results represent the mean ± SD (n = 6). **B)** The amount of methylesters in the cell wall were quantified at 24-hour post inoculation. The results represent the mean ± SD (n = 6). **C)** Quantification of lesion areas produced by the spreading of the fungus at 24 hours post infections. Data represent mean ± SE (n≥15 lesions for each genotype). **D)** Photographs showing lesion areas produced by *Botrytis* on leaves of WT and *SBT3.3-OE1* plants (left) and microphotographs showing *Botrytis* colonization revealed by trypan blue staining. Bars = 1mm. The different letters in A, C and D indicate datasets significantly different according to ANOVA followed by Tukey's test ($P < 0.05$).

Figure 7. *SBT3.3* overexpression enhances immune responces. The induction of the expression of defence genes *WRKY33, PAD3, WAK2, CYP81F2, PME17, PMEI10* were compared between *SBT3.3-OE1* line and WT plants challenged with *Botrytis*. The mRNA expression was analysed at 24 hpi in *B. cinerea*- or mock-inoculated leaves of 6-week-old *Arabidopsis* by qPCR. Botrytis *β-tubulin* expression

was also quantified. The expression levels were normalized to *Ubiquitin5* expression. The experiments were repeated three times with similar results.

Figure 8. SBT3.3 and Pro-PME17 are delivered in the apoplast through a conventional protein secretion pathway. Confocal microscopy images of epidermal cells of *Nicotiana tabacum* adult leaves showing the co-expression of SBT3.3-YFP **(A-J)** or Pro-PME17-GFP **(K-T)** with different markers of subcellular compartments (**B, L**: RFP-HDEL, endoplasmic reticulum; **E, O**: ST52-mCherry, Golgi stacks; **H, R**: XTH11-RFP, cell wall) at the indicated hours post infiltration. Plasmolyzed cells (1 M NaCl) expressing SBT3.3-YFP or Pro-PME17-GFP and the plasma membrane marker pm-rk show the green fluorescent cell wall and the retracted red fluorescent plasma membrane (**J, T**). Scale bars = 10 µm (**A-F**), 20 µm (**G-I, M-S**), and 5 µm (**J, T**).

Figure 9. Pro-PME17 and SBT3.3 colocalize in the cell wall and their colocalization is favoured over time. Confocal microscopy images of epidermal cells of tobacco adult leaves co-expressing Pro-PME17-RFP **(A and B)** and SBT3.3-YFP **(C and D)** at the indicated hours post transformation. Merged images showing the co-localization of SBT3.3-YFP and Pro-PME17-RFP in the cell wall. Overlap coefficient (OC, after Manders) and R (Pearson's correlation coefficient) values are reported in each merged image. Chlorophyll auto-fluorescence within the chloroplasts is depicted in blue. Scale bars = 20 µm

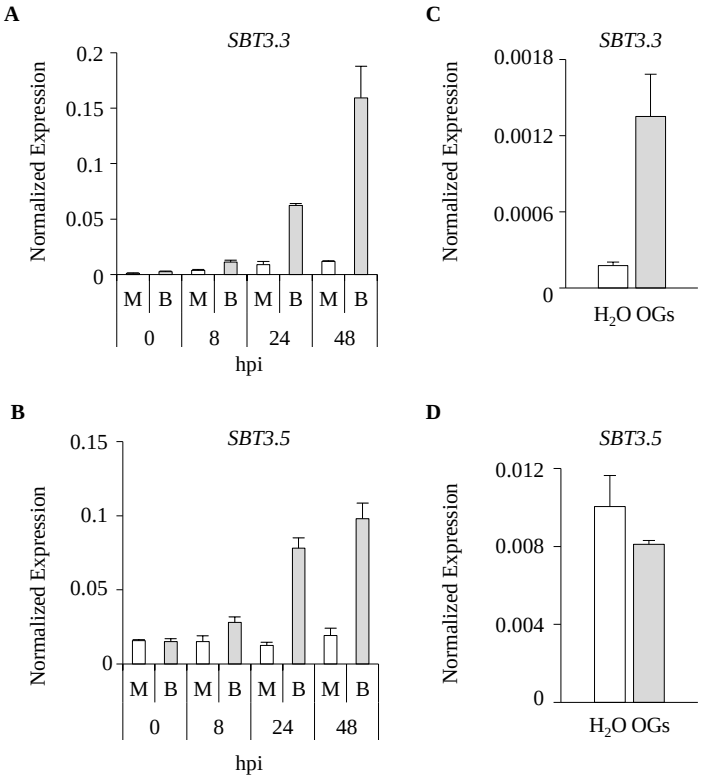

Figure 1. *SBT3.3* and *SBT3.5* are induced in *Arabidopsis* during *B. cinerea* infection and SBT3.3 is induced by OGs treatment. A) *SBT3.3* and B) *SBT3.5* expression was analysed in *B. cinerea* infected or mock-inoculated leaves at the indicated hours post inoculation (hpi) by qPCR. M = Mock inoculated leaves. B = *B. cinerea* inoculated leaves. The expression of **C)** *SBT3.3* and **D)** *SBT3.5* was analysed in Arabidopsis WT seedlings after 1 hour of treatment with OGs or with water (H_2O) as a control. The expression levels were normalized to *Ubiquitin5* expression. Data represent mean ± SD (n=3). The experiments were repeated three times with similar results.

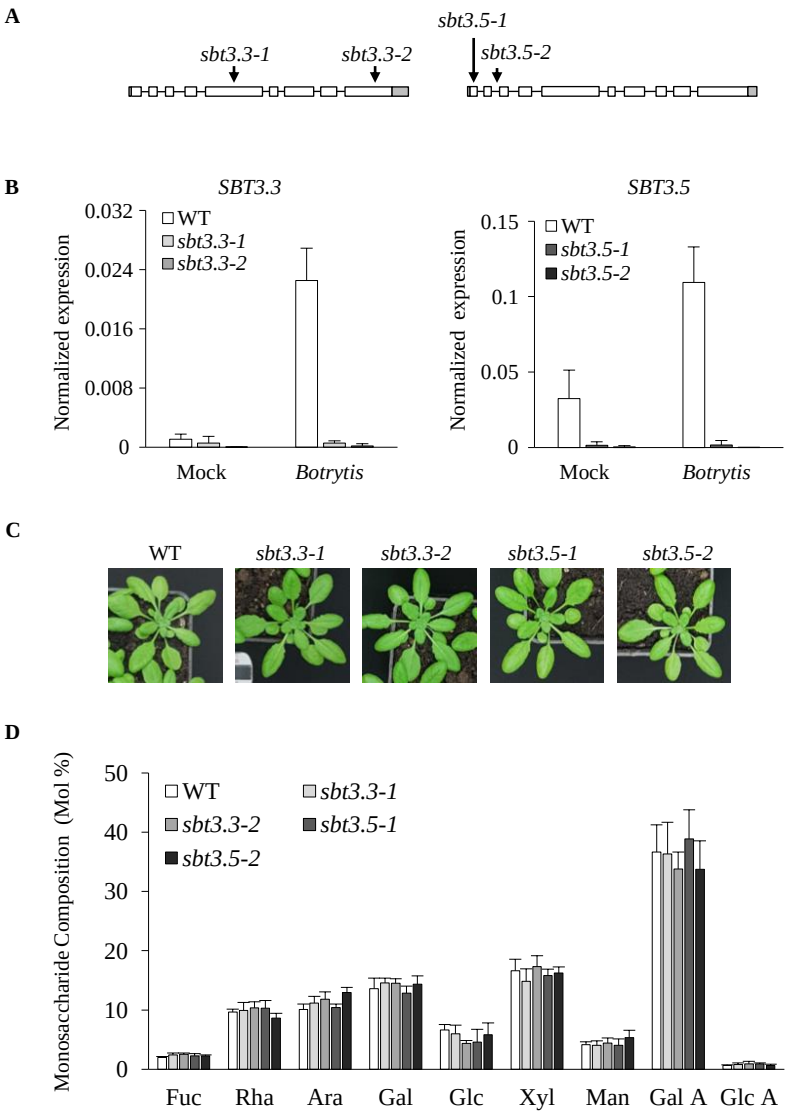

Figure 2. Isolation of Arabidopsis *SBT3.3* and *SBT3.5* T-DNA insertional mutants. A) Schematic representation of *SBT3.3* and *SBT3.5* gene structures. The localization of T-DNA insertions in the gene sequences are shown (black arrows). 5′-UTR and 3′-UTR are represented in grey, exons in white and introns as a black line. **B)** The expression of *SBT3.3* and *SBT3.5* was analyzed in the respective mutants and WT plants at 24-hour post inoculation with *B. cinerea*. The expression levels were normalized to *Ubiquitin 5* expression. The experiments were repeated three times with similar results. **C)** Representative pictures illustrating the morphology of vegetative rosettes (four-weeks old plants) of *sbt3.3* and *sbt3.5* mutants compared with WT. **D)** The monosaccharide composition of cell wall matrix polysaccharides was compared in leaves of *sbt3.3* and *sbt3.5* mutants and WT plants. The molar percentages of Fucose (Fuc), Rhamnose (Rha), Arabinose (Ara), Galactose (Gal), Glucose (Glu), Xylose (Xyl), Mannose (Man), Galacturonic Acid (Gal A) and Glucuronic Acid (Glc A) were quantified. The results represent the mean ± SD (n≥3). Monosaccharide datasets are not significantly different according to analysis of variance (ANOVA) followed by Tukey's test ($P < 0.05$).

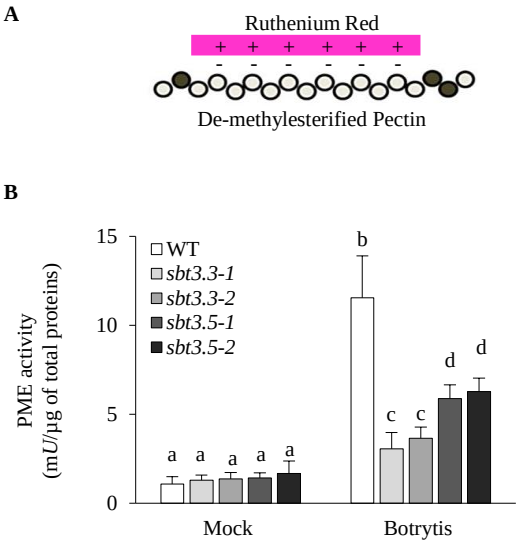

Figure 3. SBT3.3 and SBT3.5 regulate PME activity during disease. A) Schematic representation of the binding of Ruthenium Red to de-methylesterified pectin. **B)** Leaves of Arabidopsis WT and of *sbt* mutants were inoculated with *Botrytis* and Mock and PME activity were quantified at 24-hour post inoculation (hpi). The results represent the mean ± SD (n = 6). The different letters on the bars indicate datasets significantly different according to ANOVA followed by Tukey's test ($P < 0.05$).

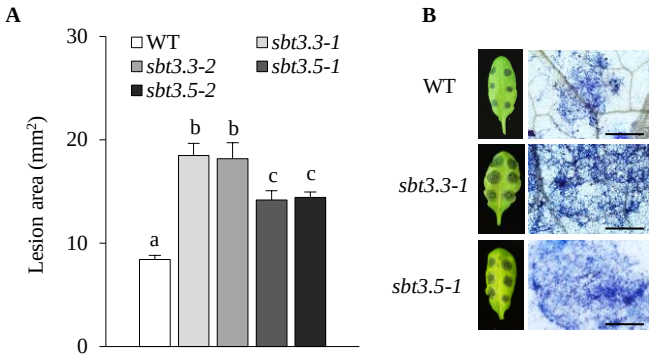

Figure 4. The lack of *SBT3.3 and SBT3.5* expression reduces *Arabidopsis* resistance to *Botrytis cinerea*. A) Quantification of lesion areas produced by the spreading of the fungus at 24 hours post infections. Data represent mean ± SE (n ≥14 lesions for each genotype). Different letters indicate statistically significant differences, according to ANOVA followed by Tukey's significance test ($P < 0.05$). **B)** Photographs showing lesion areas produced by *Botrytis* on leaves of Arabidopsis WT, *sbt3.3-1 and sbt3.5-1* mutants (left) and microphotographs showing *Botrytis* colonization revealed by trypan blue staining (right). Bars = 1mm.

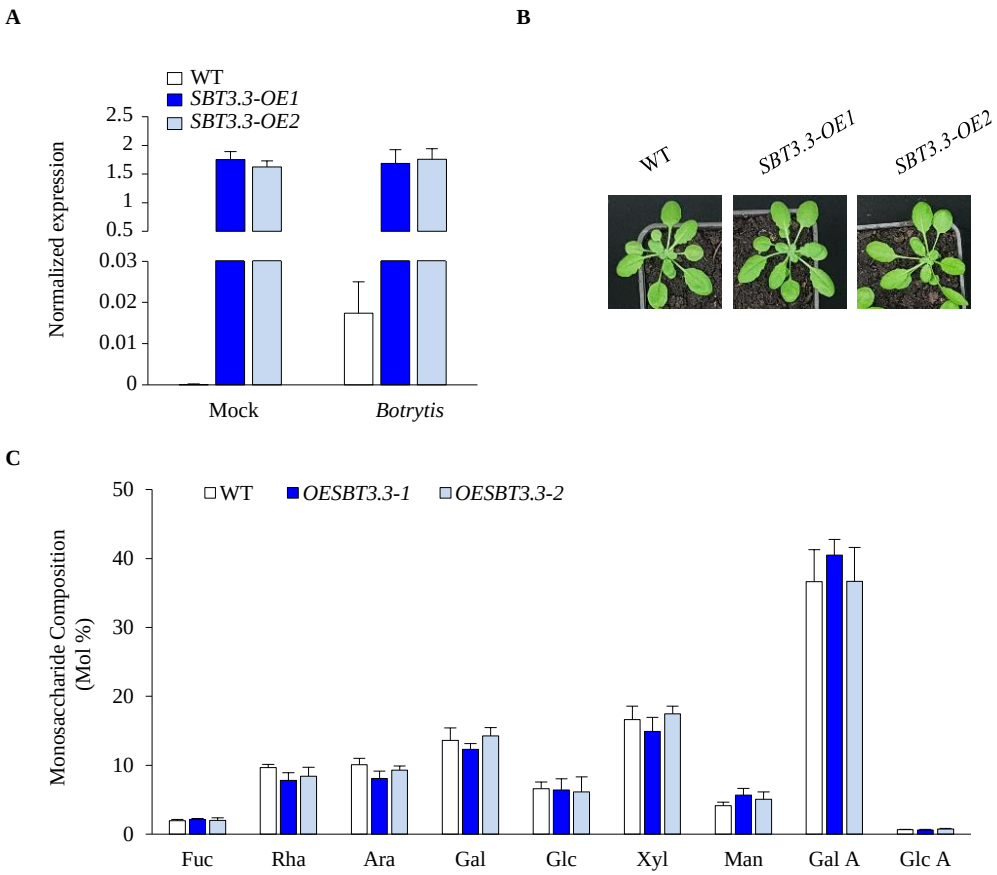

Figure 5. The *SBT3.3* overexpression in Arabidopsis does not alter rosette growth and cell wall composition. A) The expression of *SBT3.3* was analyzed in the *SBT3.3-OE1* and *SBT3.3-OE2* transgenic plants at 24-hour post inoculation with Mock and *B. cinerea* spores. The expression levels were normalized to *Ubiquitin5* expression. The experiments were repeated three times with similar results. **B)** Representative pictures illustrating the morphology of vegetative rosettes of *SBT3.3* overexpressing plants compared with WT plants. **C)** The molar percentages of Fucose (Fuc), Rhamnose (Rha), Arabinose (Ara), Galactose (Gal), Glucose (Glu), Xylose (Xyl), Mannose (Man), Galacturonic Acid (Gal A) and Glucuronic Acid (Glc A) were quantified. The results represent the mean ± SD ($n \geq 3$). Monosaccharide datasets are not significantly different according to analysis of variance (ANOVA) followed by Tukey's test ($P < 0.05$).

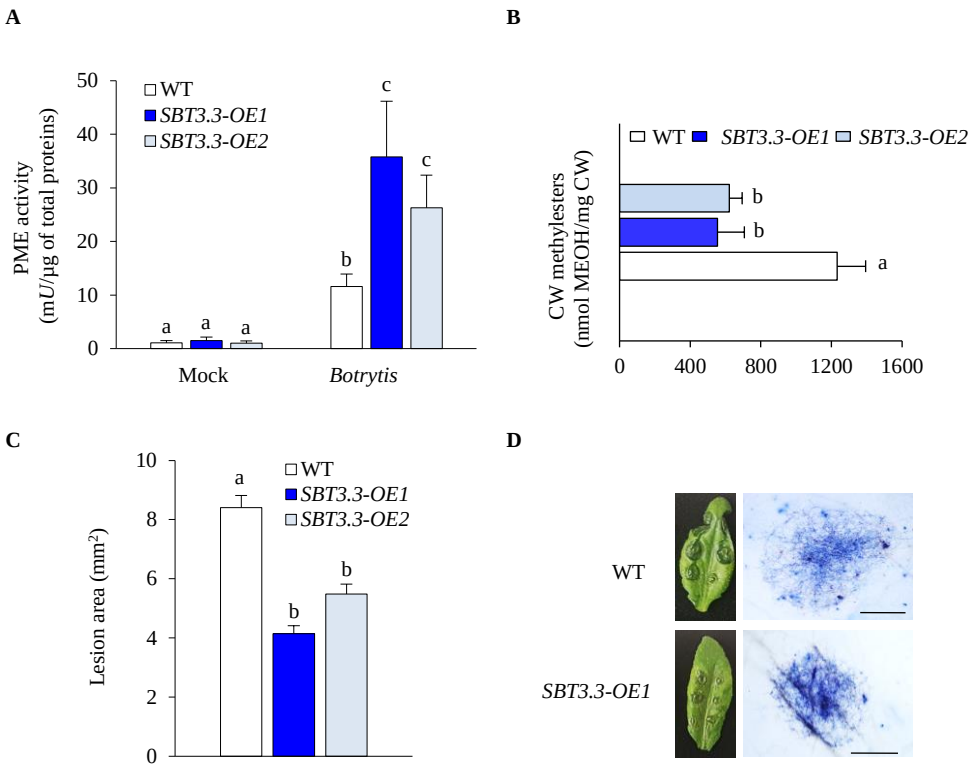

Figure 6. The *SBT3.3* overexpression overactivates PME activity restricting *Botrytis* infection. A) Leaves of Arabidopsis WT and of *SBT3.3-OE* plants were inoculated with *Botrytis* and Mock and PME activity were quantified at 24-hour post inoculation. The results represent the mean ± SD (n = 6). **B)** The amount of methylesters in the cell wall were quantified at 24-hour post inoculation. The results represent the mean ± SD (n = 6). **C)** Quantification of lesion areas produced by the spreading of the fungus at 24 hours post infections. Data represent mean ± SE (n≥15 lesions for each genotype). **D)** Photographs showing lesion areas produced by *Botrytis* on leaves of WT and *SBT3.3-OE1* plants (left) and microphotographs showing *Botrytis* colonization revealed by trypan blue staining. Bars = 1mm. The different letters in A , C and D indicate datasets significantly different according to ANOVA followed by Tukey's test ($P < 0.05$).

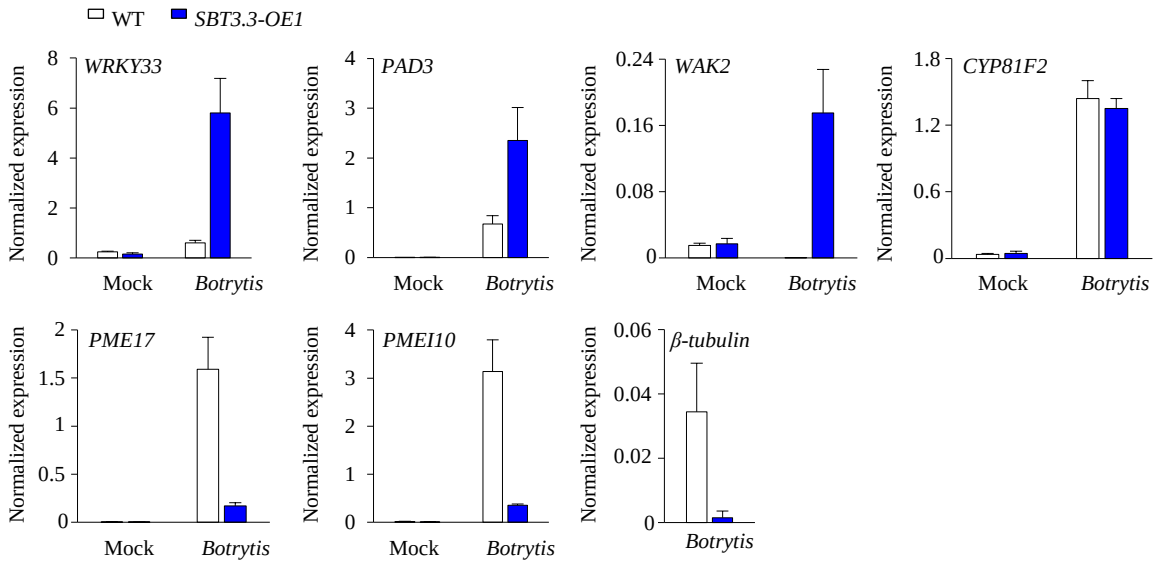

Figure 7. *SBT3.3* overexpression enhances immune responces. The induction of the expression of defence genes *WRKY33, PAD3, WAK2, CYP81F2, PME17, PMEI10* were compared between *SBT3.3-OE1* line and WT plants challenged with *Botrytis*. The mRNA expression was analysed at 24 hpi in *B. cinerea*- or mock-inoculated leaves of 6-week-old *Arabidopsis* by qPCR. Botrytis *β-tubulin* expression was also quantified. The expression levels were normalized to *Ubiquitin5* expression. The experiments were repeated three times with similar results.

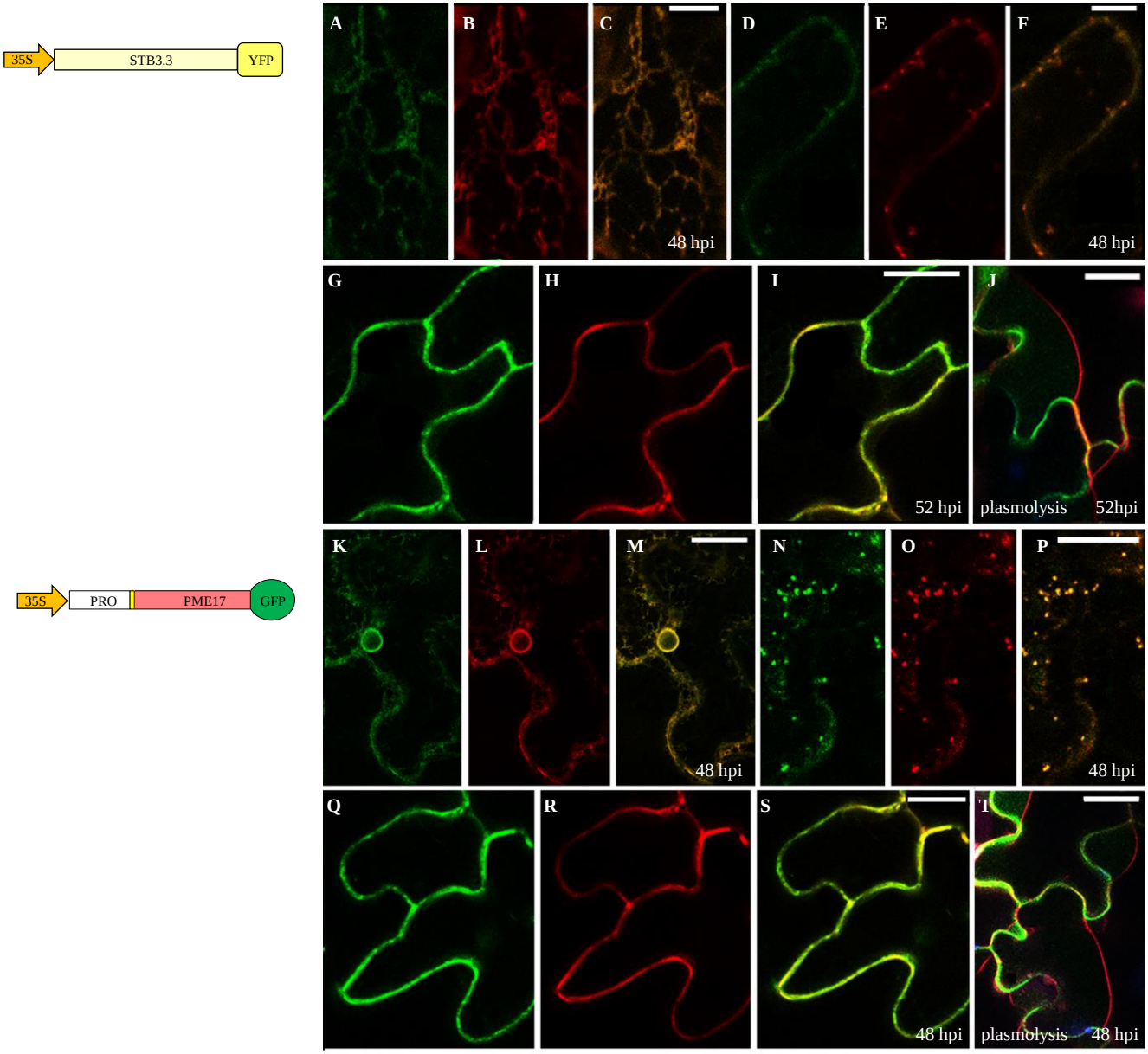

Figure 8. SBT3.3 and Pro-PME17 are delivered in the apoplast through a conventional protein secretion pathway. Confocal microscopy images of epidermal cells of *Nicotiana tabacum* adult leaves showing the co-expression of SBT3.3-YFP **(A-J)** or Pro-PME17-GFP **(K-T)** with different markers of subcellular compartments (**B, L:** RFP-HDEL, endoplasmic reticulum; **E, O**: ST52-mCherry, Golgi stacks; **H, R**: XTH11-RFP, cell wall) at the indicated hours post infiltration. Plasmolyzed cells (1 M NaCl) expressing SBT3.3-YFP or Pro-PME17-GFP and the plasma membrane marker pm-rk show the green fluorescent cell wall and the retracted red fluorescent plasma membrane (**J, T**). Scale bars = 10 µm **(A-F)**, 20 µm (**G-I, M-S**), and 5 µm **(J, T).**

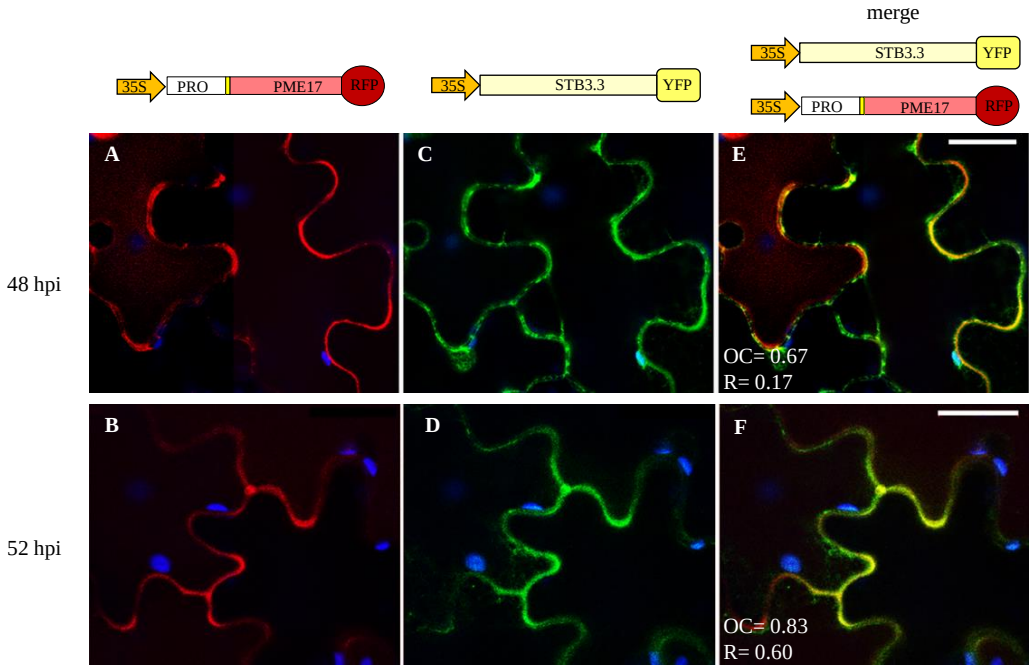

Figure 9. Pro-PME17 and SBT3.3 colocalize in the cell wall and their colocalization is favoured over time. Confocal microscopy images of epidermal cells of tobacco adult leaves co-expressing Pro-PME17-RFP **(A and B)** and SBT3.3-YFP **(C and D)** at the indicated hours post transformation. Merged images showing the co-localization of SBT3.3-YFP and Pro-PME17-RFP in the cell wall. Overlap coefficient (OC, after Manders) and R (Pearson's correlation coefficient) values are reported in each merged image. Chlorophyll auto-fluorescence within the chloroplasts is depicted in blue. Scale bars = 20 µm